OPTIMISATION OF LASER PARAMETERS FOR TREATMENT OF BASAL CELL CARCINOMA

Nakul Dewan

OPTIMISATION OF LASER PARAMETERS FOR TREATMENT OF BASAL CELL CARCINOMA

Thesis submitted to the
National Institute of Technology, Rourkela
for the award of the degree

of

Master's of Technology in Biomedical Engineering

by

Nakul Dewan

Under the guidance of

Dr. Amitesh Kumar

DEPARTMENT OF BIOTECHNOLOGY & MEDICAL ENGINEERING

NATIONAL INSTITUTE OF TECHNOLOGY, ROURKELA

JUNE 2013

CERTIFICATE

This is to certify that the thesis entitled **Optimisation of Laser Parameters for Treatment of Basal Cell Carcinoma**, submitted by **Nakul Dewan** to National Institute of Technology, Rourkela, is an authentic record of bona fide research work carried under my supervision and I consider it worthy of consideration for the award of the degree of Master's of Technology of the Institute.

Date :

Dr. Amitesh Kumar
Assisstant Professor
Department of Biotechnology & Medical Engineering
National Institute of Technology
Rourkela, 769008

DECLARATION

I certify that

1. The work contained in the thesis is original and has been done by myself under the general supervision of my supervisor.
2. The work has not been submitted to any other Institute for any degree or diploma.
3. I have followed the guidelines provided by the Institute in writing the thesis.
4. Whenever I have used materials (data, theoretical analysis, and text) from other sources, I have given due credit to them by citing them in the text of the thesis and giving their details in the references.

Nakul Dewan

CURRICULUM VITA

Name: Nakul Dewan

Educational Qualification:

Year	Degree	Subject	University
2011	B.Tech(honours)	Biotechnology	L.P.U., Jalandhar

List of Conference Publications:

1. Dewan, N., Kumar, A., "Effect of anisotropy and Scattering Coefficient on Light Distribution in a semi-infinite tissue" in ICMSDPA-2012 at B.H.U., Varanasi.

2. Dewan, N., Kumar, A., "Effect of Different Laser Beam Profiles on Thermal Damage of Basal Cell Carcinoma" in BEATS-2012 at NIT Jalandhar.

ACKNOWLEDGEMENTS

We dream, we desire, we strive to achieve our dreams, at last it is our perseverance and determination that pays and then only we achieve what we dream. So, today it is my dream that I am at the meridian of achieving my goal. As I begin to write these lines; after completion of my thesis, my heart is filled with deepest sense of gratitude. I shall ever remain thankfully indebted to all those who have directly or indirectly encouraged me to achieve my goal and enlightened me with the touch of their cognizance and encouragement.

First and foremost, I consider it as a blessing to pursue my Project under the able guidance of Dr. Amitesh Kumar, whose insights and approvals have contributed so much to this thesis. No words are enough to express my gratitude to my mentor for his whole hearted, unflinching encouragement, meticulous supervision and support. He would take a great concern in troubleshooting problems and was always full of encouraging words. His words of applause and sincere criticism in the last one year helped me a lot to develop my ideas regarding many important issues in life.

I always believed that a cheerful lab atmosphere is the key to productivity. I am indebted to my lab mates for providing a stimulating and relaxed environment. I would like to pay sincere regards to Mr. Karan Bhatt who was unending in his expertise, support & encouragement and always stood on his toes to help me.

No task is difficult if you have a friend like Mr. Om Shankar Awasthy who was the greatest help I could have dreamt of. You provided such wonderful company and made my stay in N.I.T, Rourkela a pleasant experience. We had such memorable time in this institute that it's painful to note that we will be moving to new places. Thanks a million, for being with me, whenever I needed any help. I will remember the wonderful time we had for a long time to come.

Where emotions are involved words cease to mean, lexicon could not have the words to express the affection, blessings, encouragement, sacrifice and love of my beloved Mother, Father, Brother and Sister-in-law without which I would have never come to this proliferative stage and engaged myself in career building. Last and above all, having such a wonderful family that supports me whole heartedly, no matter what I do, is something I feel unique to my life. There are no words to pay regards to them for toiling so hard to bring me up to this stage.

At last, I would like to express my deep sense of gratitude to almighty GOD, many known and unknown hands which pushed me forward.

Date :
Place :

Nakul Dewan

Contents

List of Figures

List of Tables

LIST OF SYMBOLS AND ABBREVIATIONS

A	frequency factor (1/s)
c	specific heat (J/kg K)
c_b	specific heat of blood (J/kg K)
D	tumour depth (mm)
E_a	burn activation energy (J /mole)
g	anisotropy of tissue
g_{epi}	anisotropy of epidermis
$I(r,z)$	intensity of laser light at position r in the z direction (W/m^2)
k	thermal conductivity of tissue (W/m K)
P	power of laser (W)
q	heat flux (W/m^2)
r	coordinate variable in the radial direction (m)
R_l	laser beam radius (mm)
R_t	tumour radius (mm)
S	source term due to laser light absorption in the tissue (W/m^3)
T	temperature (K)
T_0	initial temperature of tissue (K)
T_b	temperature of blood (K)
T_{max}	maximum temperature (K)
t	time (s)
$t_{Irradiation}$	irradiation time (s)
$\dot{w}_b$	blood perfusion rate (m^3/m^{3}tissues)
W	water mass content
z	coordinate variable in the axial direction (m)
z_t	thickness of the tissue (m)

Greek Letters

f_{mel}	volume fraction of melanosome in epidermis
f_{blood}	volume fraction of blood
γ	attenuation coefficient (cm^{-1})
μ_a	absorption coefficient (cm^{-1})
μ_s	scattering coefficient (cm^{-1})
$\mu_{a.epi}$	net epidermal absorption coefficient (cm^{-1})
$\mu_{a.skinbaseline}$	baseline absorption coefficient of melaninless epidermis and bloodless dermis (cm^{-1})
$\mu_{a.mel}$	absorption coefficient of single melanosome (cm^{-1})
$\mu_{a.derm}$	absorption coefficient of dermis with perfused blood (cm^{-1})
$\mu_{a.blood}$	absorption coefficient of blood (cm^{-1})

$\mu_{a.subfat}$	absorption coefficient of subcutaneous fat (cm^{-1})
$\mu_{s.epi}$	scattering coefficient of epidermis (cm^{-1})
$\mu_{s.derm}$	scattering coefficient of dermis (cm^{-1})
$\mu_{s.subfat}$	scattering coefficient of subcutaneous fat (cm^{-1})
$\mu_{sp.epi}$	reduced scattering coefficient due to epidermis (cm^{-1})
$\mu_{sp.derm}$	reduced scattering coefficient due to dermis (cm^{-1})
$\mu_{sp\_Mie.fibers}$	Mie scattering component due to large cylindrical dermal collagen fibers (cm^{-1})
$\mu_{sp\_Rayleigh}$	Rayleigh scattering component due to small structures associated with collagen fibers (cm^{-1})
Ω	tissue damage integral
ρ	density of tissue (kg/m^3)
ρ_b	mass density of blood (kg/m^3)

ABSTRACT

In this study a model is proposed to estimate and optimise the exposure durations of laser beams of different powers for superficial Basal Cell Carcinomas of varying radii and depth. The frequent application of Laser in medical field makes it a matter of significance, to study the distribution of temperature in tissue, its effects on tumourous tissue and the extent of thermal damage in healthy tissue during photo-thermal therapy. The tissue temperature is numerically estimated by solving Penne's bioheat equation for 2-D multilayered skin model using Finite Volume Method and the conversion of laser light inside the tissue is expressed by Beer-Lambert's Law. This study focuses on Basal Cell Carcinoma (BCC) which is a semi-malignant tumour of the skin that derives from incompletely differentiated immature keratinocytes of the epidermis. In this paper, different sizes of Basal Cell Carcinoma are considered which are irradiated by continuous wave Nd:YAG laser with Gaussian beam profile. The spatial and temporal thermal damage to the tissue is estimated by using the Henriques' theory of skin burns which uses Arrhenius equation. A hitherto unused grid-based model is employed to depict the penetration of the damage front viewed against the tumour-tissue interface. This study attempts to propose a correlation between optimised exposure time and laser power for a particular tumour radius. An inverse proportional relation between laser power and irradiation time, for a particular tumour radius, was quantitatively established in this study.

Keywords: Basal cell carcinoma, Bio-heat equation, Finite volume method, Thermal damage, Hematocrit value, Laser

CHAPTER 1

Introduction

The complications of surgery in the case of localised diseases can be overcome by an alternate technique, i.e. ablation that has several advantages over conventional techniques. Research work has been going on to find techniques that are completely non-invasive, or minimally so, with the objective of producing efficient results while reducing the risk of complications. The real-time monitoring is significant during the necrosis of a tumour so as to ensure complete tumour necrosis with minimal healthy tissue damage. For this, localised destruction of tumours becomes a paramount thing which can be achieved by using heat treatment locally. The use of heat energy for treatment purposes has existed since ancient times. The cauterisation of breast tumours with glowing rods is described on a 5000 year old Egyptian papyrus roll. The infection of malignant tumours with pyrogenic bacteria, resulting in its retrogradation, has been described in the reports since the start of the 20^{th} century [7]. The differentiation between the effects of heat and immunological responses became difficult in fever-inducing treatments which led to further exploration into the methods of using heat for tumour therapy.

Some of the studies that have been carried out in this field suggest the therapeutic activity of heat on penile and uterine carcinomas as well as the adjuvant quality of heat therapy that helps in increasing the efficiency of other therapeutic modalities like radiotherapy [8]. Localised heat treatment with radiation therapy is used to treat recurrent breast cancer, cervical nodal metastases from head and neck cancers and superficial, metastatic or recurrent malignant melanoma [9].

In tumour therapy, heat is generally applied with the objective of increasing the temperature of the tissue by only a few degrees in order to make the tumours more sensitive to ionising radiation and certain drugs. At hyperthermic temperatures ($41^o - 47^oC$), an increased heat sensitivity of tumours over normal tissues has been observed. This

potential benefit is difficult to fully explore clinically because of technical problems in delivering uniform heating to deep tumour sites even though the techniques for heat delivery have been refined since the use of glowing irons. Whole body and regional heat treatment by heated blood limits the temperatures that can be attained because of the limits of patient tolerance.

When applied at higher temperatures, above approximately 50^oC, the treatment is termed thermotherapy. Thermotherapy speeds up tissue necrosis. At these temperatures, no selectivity in heat sensitivity exists between tumorous and normal tissues. Therefore, accuracy is important while determining the region that needs thermotherapy, because whatever tissue is heated, is necrosed. One of the sources for the induction of local temperature rise in tissue can be Laser light.

1.1 Laser

LASER is an acronym for (L)ight (A)mplification by (S)timulated (E)mission of (R)adiation. Many potential applications have been explored after Theodar Maiman submitted the first report on laser radiation in 1960 [10]. To overcome the inherent limitations of conventional medical therapeutic techniques, biologists and physicians have been involved in designing novel methods in which laser light could be used with efficacy. The first applications of lasers were observed in ophthalmology. The outcome of Meyer-Schwickerath's study which suggested the coagulative effect of xenon flash lamp on retinal tissue and the high transparency of eye, making the interior organs easily exposed, was the reason behind the first ophthalmological application. Zaret et al. [11], conducted the study on this ophthalmological application just one year after the invention of the laser . The treatment of retinal detachment was reported by Campbell et al. [12] and by Zweng et al. [13] very soon after the report of Zaret's study. In the field of dentistry, application of lasers was initiated after the investigations carried out by Goldman et al. [14] and Stern and Sognnaes [15].

As the horizons of laser application expanded, investigations into the use of types of lasers other than the ruby laser were also began. In 1960's the application of lasers in various other medical disciplines was also introduced. There are a myriad of laser procedures performed all around the globe in today's scenario. Most of them come under the category of minimally invasive surgery (MIS), a novel approach of the present times, describing non-contact and bloodless surgical procedures. These two features of lasers are the reasons that they are tagged as universal scalpel and treatment aid. But, the treatment of some disease with a particular laser can be disastrous for another type of disease, if the same laser is used. The usability of laser for a particular disease or site of treatment also varies with the parameters used, with the wrong parameters having the possibility of having disastrous consequences. For example, heat treatment of cancer-

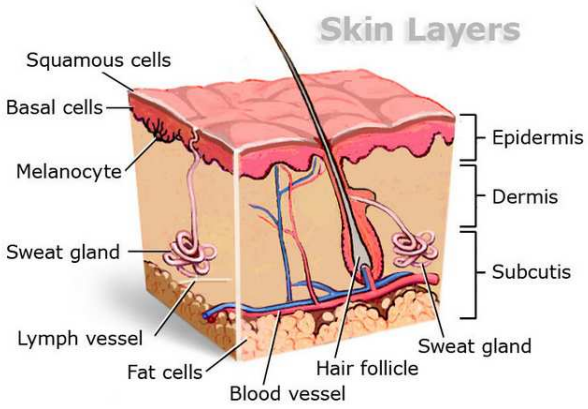

Figure 1.1: Schematic diagram of layered structure skin with many small structure embedded. Adapted from [1]

ous tissue to cause thermal necrosis whereas if the same parameters are used for retinal coagulation can burn the retina leading to irreversible blindness. So, the application of lasers becomes specific for specific target sites.

Lasers can be broadly categorised as continuous wave (CW) lasers and pulsed lasers. Continuous wave lasers include most gas lasers and to some extent some solid-state lasers also, while pulsed lasers includes solid-state lasers, excimer lasers, and certain dye lasers. The first important parameter in case of pulsed laser is pulse duration as it decides the type of interaction with the biological tissue. The second parameter, wavelength, is also a significant factor which decides the penetration depth of the laser radiation. Third parameter, energy density, is only required as a necessary condition for the occurrence of a certain effect and it determines its extent [10]. Fourth parameter, applied intensity, is defined as the ratio of applied energy to pulse duration. Two recent laser developments which have become more and more important for medical research include: diode laser and free electron laser. The progress in laser surgery can primarily be attributed to the fast evolution of pulsed laser systems as it is the pulse duration which determines the effect on biological tissue.

1.2 Skin

Skin is the largest organ of the human body with area of approximately $2m^2$ and weight $5Kg$. It consists of two separate layers: the outer epidermis and the inner dermis. Below the dermis lies the subcutaneous fat, which is the innermost layer. This layer is composed of proteins and adipose tissue, but it is usually not considered as a part of the skin [16], as illustrated in figure 1.1.

The outer epidermis is further divided into four to five layers. They collectively make around $100\mu m$ of thickness of this entire layer. The peripheral layer is made up of keratinocytes, which produce fibrous protein named keratin. This layer covers 90% of the

epidermis. The younger cells make up the deeper layers of epidermis and they transform into hard protective layer gradually along the way towards periphery. The other type of cells that are present in between keratinocytes are melanocytes which are responsible for the production of the pigment melanin. Melanin contributes strongly in the absorption of light into the skin. These melanocytes are present in the form of packets which are known as melanosomes which are of $1-2\mu m$ diameter. Apart from melanin synthesis, melanosomes also help in protecting keratinocytes from UV light coming from the Sun. The melanosome concentration slightly differs in humans but the amount of melanin synthesis differs drastically. The distribution pattern of melanosomes can also vary which is why there are freckles, patches, age spots and different skin colours in different individuals [16].

The inner layer, dermis, is thicker (up to $\sim 1mm$). This layer is adequately supplied with blood and nerves. This layer constitutes of two proteins: collagen and elastin. These two proteins help in providing strength and elasticity to the skin. Along with these two proteins, there are other structures like tiny loops of blood that help in regulating body temperature, glands, receptors for various stimuli, and hair follicles. Hair from the hair follicles are made up of keratin protein and colour is provided by the melanin. Due to the concentration of cutaneous blood in venous plexus in dermis, which is $100-200\mu m$ from the surface, the absorption of light mainly occurs because of hemoglobin, unlike in epidermis where blood is not present in adequate amount [16].

1.2.1 Skin optics

The components that contribute towards absorption in biological tissues are water molecules, proteins and pigments [17]. The absorption of light by tissue results in the reduction of light intensity with increase in depth. According to Beer-Lambert's Law:

$$I(z;\lambda) \propto e^{-\mu_a(\lambda)z} \tag{1.1}$$

where absorption coefficient,μ_a, is dependent on the wavelength.

The absorption spectra in figure 1.2 depicts that the water absorbs strongly above $2\mu m$, with the strongest peak occurring at $3\mu m$; proteins strongly absorb in UV range ($280nm$) and pigments contribute for absorption mostly in visual and Near-Infrared (NIR) range, i.e. $400-2000nm$. The absorption coefficient of skin varies in different individuals because of different melanosome concentrations. For Caucasians, the absorption coefficient at Nd:YAG wavelength is approximately $0.1cm^{-1}$.

Skin also contributes to another phenomenon called scattering. The value of scattering coefficient for skin lies in between $10-100cm^{-1}$. There are two types of scattering that occur inside tissue owing to two distinct type of structures. The first type is called

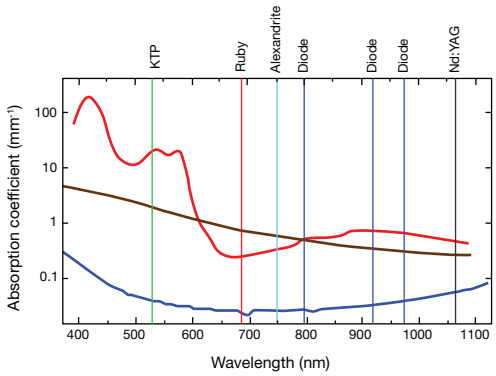

Figure 1.2: Absorption spectra of the skin's main absorbents: water (blue), melanin (brown), hemoglobin (red). Taken from [2]

Rayleigh scattering which is contributed by scattering of atoms and molecules, where the Intensity of scattering, I_s, is inversely proportional to the fourth power of light's wavelength:

$$I_s \propto \frac{1+cos^2\theta}{\lambda^4} \tag{1.2}$$

where θ is the deflection angle.

The second type is called Mie scattering which is contributed by the collagen fibers and other structures which have sizes similar to light's wavelength. The wavelength dependence of this scattered intensity is very less:

$$I_s \propto \lambda^{-x} \tag{1.3}$$

where x is in between $0.4-0.5$, and the scattering is mostly in the forward direction. The introduction of many empirical scattering functions has been done to fit the measured data and explain the angular probability after the scattering "event". These functions can be used to predict the probability of the scattering event and to monitor the propagation of light through the skin or other tissues [18].

1.2.2 Basal Cell Carcinoma and its Histological types

Basal Cell Carcinoma (BCC) is defined by the World Health Organisation Committee on the histological typing of skin tumours as a locally invasive, slowly spreading tumour which rarely metastasizes, arising in the deepest layer of epidermis or hair follicles and in which, in particular, the peripheral cells usually simulate the basal cells of the epidermis [19]. It is the most common form of cancer in the United States [20], with about

900,000 people being diagnosed (550,000 male, 350,000 female) every year. The estimated lifetime risk of basal cell carcinoma in the white population is $17-39\%$ for men and $15-28\%$ for women [21]. The superficial BCC accounts for $10-15\%$ of all BCC cases, and it is frequently reported in younger age categories [22]. This kind of carcinoma consists of small islets of basaloid tumour cells which have well defined boundaries against the normal epithelia. The superficial lesions are often found on the trunk and the extremities although the site of occurrence is mostly head and neck, accounting for around 40% [23] of the cases. BCC is usually observed in older patients who are frequently and intensively exposed to the ultraviolet radiation during the course of their lives.

The growth of BCC is characteristically slow and it takes months and sometimes years to evolve. The tissue which actively divides remains at the periphery of the lesion and at the center of the lesion apoptosis occurs that leads to ulceration. The strategy to treat these carcinomas is to eliminate the tissue from the farthest marginal areas as these cells have a very aggressive behaviour. These cells can grow slowly and steadily for years and invade bones as well as soft tissues. There is a predilection for invasion along tissue planes, the periosteum, and nerves. A common theory states that the embryonic fusion planes, such as the nasolabial fold, are more susceptible to tumor growth [24].

BCC is characterised by large oval-shaped nuclei comprised majorly of cellular matrix with a little cytosol. The nucleus-to-cytoplasm ratio is higher in these cells as compared to normal cells. The nulcei form a picket fence-type arrangement in peripheral cells which enclose the tumourous mass. Histological types of BCC are as follows:

1. Nodular BCC
2. Superficial multifocal BCC
3. Morpheaform BCC
4. Infiltrating BCC
5. Metatypic BCC
6. Fibroepithelial of Pinkus [25].

1.3 Light and Matter

The photons of the laser light can either be absorbed or unabsorbed when impinged on the tissue. The unabsorbed light can undergo two processes, i.e. it can either be transmitted from the other side or else it can get re-emitted. During the travel inside the tissue, light can change its direction due to scattering or it can move along the previous path. Hence, there are four phenomena which occur when biological tissue is exposed

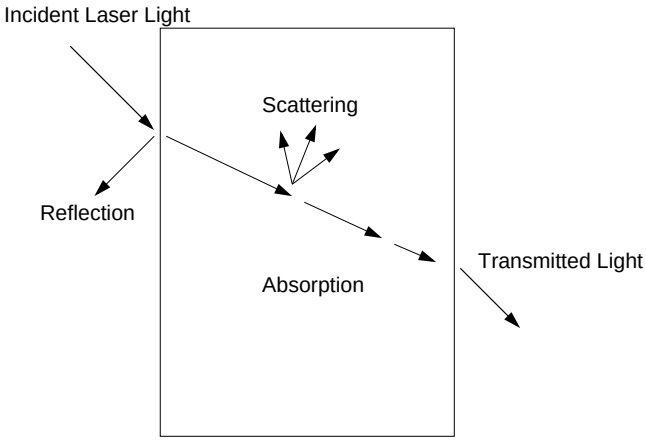

Figure 1.3: Geometry of reflection, refraction, absorption, and scattering. Adapted from [3].

to the laser light: reflection, scattering, absorption and transmittance, as shown in figure 1.3.

The reflection of the laser light is governed by Fresnel's Law. The factors on which the interaction of light with tissue depends are: properties of incident light and optical properties of tissue, which govern the propagation of light [18].

Remission occurs when the light reflects from the front or scatters and passes through the interface leaving the tissue. Scattering of light occurs when it interacts with the tissue (fluctuation in index of refraction) and changes direction, without changing the wavelength. Absorption of a photon takes place only when its energy corresponds to the energy difference between such quantised states as:

$$E = h\upsilon \tag{1.4}$$

Absorption of light in tissue induces changes in the energy state from the ground state to the excited state, which drives a number of chemical processes.

1.3.1 Interaction of Laser with tissue

There are several possible events that may take place on the application of laser light to the biological tissue. Since the invention of the laser, researchers have been exploring its potential interaction effects by exploiting every available laser system and tissue target. Even though the number of combinations for the experimental parameters is infinite, there are five categories of interaction mechanisms as follows:

1. Photo chemical Interactions

2. Thermal Interactions

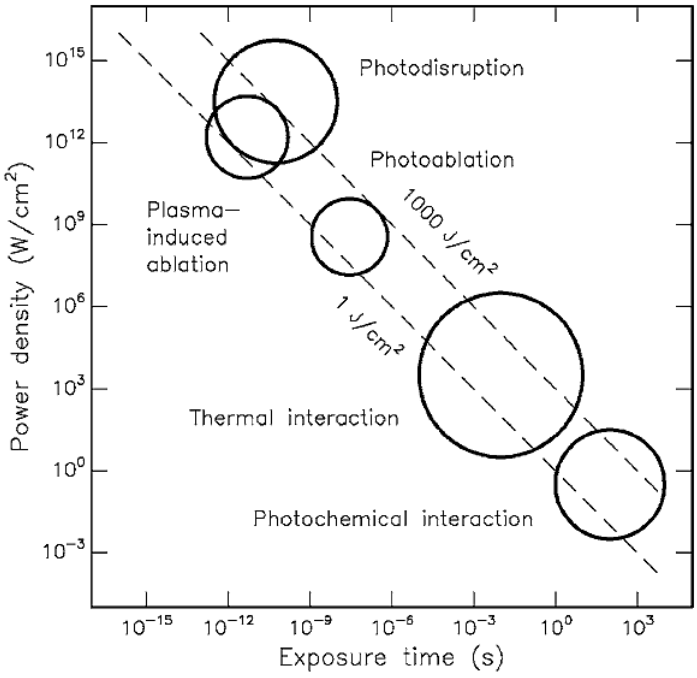

Figure 1.4: Map of laser-tissue interactions. The circles give only a rough estimate of the associated laser parameters. Modified from [4]

3. Photo ablation
4. Plasma-induced ablation
5. Photo disruption

These interaction types appear different from each other but interestingly they share a single common parameter: the characteristic energy density ranges from approximately $1\,J/cm^2$ to $1000\,J/cm^2$. A surprising fact is that power varies over 15 orders of magnitude [4]. The five basic interaction types which were found during many experiments are plotted in a double logarithmic map illustrated in figure 1.4.
The ordinate expresses the applied power density or irradiance in W/cm^2, the abscissa represents the exposure time in seconds. Two diagonals represent constant energy fluences at $1\,J/cm^2$ and $1000\,J/cm^2$, respectively [5]. There are five possible sections for doing time scaling: CW/exposure time > $1s$ for photo chemical interaction, $1min$ down to $1\mu s$ for thermal interactions, $1\mu s$ down to $1ns$ for photo ablation, and < $1ns$ for plasma-induced ablation and photo disruption. The total energy density suitable for medical laser applications ranged between $1\,J/cm^2$ to $1000\,J/cm^2$ as depicted in the figure 1.4.

1. Photo chemical Interaction: The category of photo chemical interactions originates from factual observations that chemical effects are induced by light in macromolecules or biological tissue. This type of interaction plays a significant role in field medical laser during photodynamic therapy (PDT). Although it is not yet confirmed, bio stimulation is characterised as a photo chemical interaction. At very

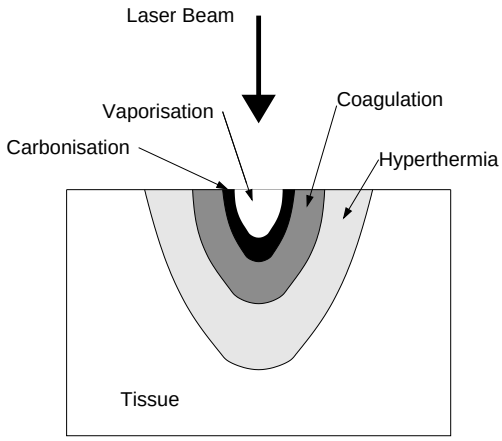

Figure 1.5: Location of thermal effects inside biological tissue. Modified from [5]

low power densities (typically $1\,W/cm^2$) and long irradiation times ranging between seconds to continuous wave, photo chemical interactions can take place. The laser parameters, if selected carefully, can lead to radiation distribution inside the tissue which can be estimated by scattering. The two properties of wavelengths in visible range (e.g. Rhodamine dye lasers at $630nm$) viz. efficiency and high optical penetration depth make them suitable for use in most cases [5]. Red dye lasers and diode lasers can be used to cause this type of interaction to occur. Photodynamic therapy and bio stimulation are two important applications of this type of interaction.

2. Thermal Interaction: The type of interactions in which rise in temperature is the important parameter change, is covered under thermal interaction. Both CW or pulsed laser radiation can be used to induce thermal effects [5]. Unlike photo chemical processes, which are controlled by a specific reaction cascade, thermal effects are considered to be nonspecific as studied in 1984 by Parrish and Deutsch [26]. There are two main factors viz. duration and peak value of the tissue, which decide the biological effects like coagulation, vaporisation, carbonisation and melting, that the tissue will undergo. The location of several thermal effects is depicted in figure 1.5. The spatial extent of each thermal effect depends on the maximum temperature achieved locally during and after the laser exposure. Typical lasers that can be used to cause this interaction type are CO_2, Nd:YAG, Er:YAG, Ho:YAG, argon ion and diode lasers. Some of the applications are thermal decomposition, treatment of retinal detachment, laser-induced interstitial thermotherapy.

3. Photo ablation: This type of interaction is basically used to precisely incise the tissue, which means to remove the tissue in a very clean and exact fashion without doing any thermal damage such as coagulation or vaporisation. In this interaction type, actual direct breaking of molecular bonds using high energy photons

takes place. Photo ablation was first discovered by Srinivasan and Mayne-Banton (1982). Photo ablation was labeled as ablative photo decomposition, i.e. the material is decomposed when exposed to high intensity laser irradiation. Excimer lasers like ArF, KrF, XeCl, XeF are used for causing this interaction type. Applications of photo ablation include refractive corneal surgery [27].

4. Plasma-Induced Ablation: This interaction type comes into play when a clean and well-defined removal of tissue, without any possibility of thermal or mechanical damage, is desired. Ablation that utilises this type of interaction is obtained by ionising plasma formation. This can be achieved if the parameters are selected appropriately. The term plasma-mediated ablation is sometimes interchangeably used with plasma-induced ablation. The investigation of Niemz et al. [28] discussed that both the analogues explain a well accepted interpretation that this kind of ablation is primarily caused by plasma ionisation itself. The lasers used for this are Nd:YAG, Nd:YLF and Ti:Sapphire. Applications of plasma-induced ablation include refractive corneal surgery and caries therapy [5].

5. Photo disruption: This type of interaction is used for fragmentation and cutting of tissue by mechanical forces. The possible processes that have been observed during this kind of interaction are plasma sparking, generation of shock waves cavitation and jet formation. The lasers that are suitable for this interaction type are solid-state lasers, e.g. Nd:YAG, Nd:YLF, Ti:Sapphire. Photo disruption was introduced by Krasnov [29] and then further explored by Aron-Rosa et al. [30] and Fankhauser et al. [31]. Since it was first introduced this type of interaction has become an important tool of minimally invasive surgery (MIS). The special applications of this type of interaction are lens fragmentation and lithotripsy.

1.4 Review of Literature

The interaction of laser with biological tissue is a subject of much interest owing to the ever-increasing role of laser in therapy. Heat therapy for treatment of skin diseases has been in use for a long time. Studies have suggested that laser radiation can be used as a source of localised heat to produce localised hyperthermia that can be utilised to produce desired changes in the target tissue, thus making it an efficient therapeutic alternative [32–34]. In addition to laser-induced hyperthermia, lasers have been widely used in clinical therapies and many other medical applications including laser-induced interstitial thermotherapy, interstitial laser photo coagulation therapy, laser microsurgery and optical imaging [35–41]. Laser therapy is widely used as a general cutting tool in dermatology, gynecology, neurology, oncology [42, 43] and many other medical fields due to desirable qualities such as increased precision and improved haemostasis which en-

sures minimal healthy-tissue manipulation. During thermal therapy, it is very important to control the temperature to prevent thermal damages in the surrounding tissue. So, computational modeling becomes essential for understanding and predicting temperature evolution and damage front propagation during laser therapy. Such an approach attempts to provide therapeutic models of increasing efficiency by optimising laser parameters in accordance with tissue parameters like the size of the tumour, and its optical and thermal properties.

Lasers are used in the treatments of the superficial tumours like basal cell carcinoma (BCC) [44]. Basal Cell Carcinoma (BCC) is a slow-growing form of skin cancer that starts from basal cells which are in the deepest layer of the epidermis. For an efficient laser therapy of BCC, the laser parameters such as power, irradiation time, spot size, energy per pulse, repetition rate, and number of pulses are optimised based on the tissue optical characteristics such as anisotropy, scattering coefficient, absorption coefficient and refractive index.

The rate of thermal distribution is estimated based on Beer-Lambert's law [45, 46]. The controlled distribution of laser energy in the tissue is important for efficient thermal therapy [47]. There have been great advancements in laser technology. Out of the many available lasers which can be explored for thermal therapy, the Nd:YAG laser has been the most frequently used in medical applications [42, 43, 48] due to its potential to stop internal haemorrhage, to treat tumours, and to cause photo-coagulation. The Nd:YAG laser can produce energy at wavelength of $1064\mu m$. When the tissue surface is exposed to laser, the tissue temperature starts to rise and phenomena like tissue coagulation, vaporisation, carbonisation, and burn occur sequentially resulting in the necrosis of tissue. In laser surgery, tissue coagulation is defined as the irreversible damage caused when temperature reaches above 60^oC up to 100^oC. If the temperature exceeds 100^oC, vaporisation and tissue ablation occur [49].

The developed model is of no significance if it is not validated by experimental results. A literature survey was carried out to determine the various models available and to compare their performances. A three step model for laser-tissue interactions was proposed by Welch [50] which included: (i) modeling of heat deposition in tissue based on the absorption coefficient (μ_a) and scattering coefficient (μ_s), (ii) determination of temperature response modeled by the heat conduction equation, and (iii) estimation of tissue denaturation. Taking it as the reference model, many other authors described these steps with some other modifications and simplifications [51]. Then a model was proposed by Takata [52] that predicted transient temperature and thermal damage. This model considered tissue modifications and steam blister formation. The results obtained from experiments conducted on pig skin using CO_2 laser validated the model. A model was developed by Halldorson and Langerholc [53] which considered modification of tissue properties after coagulation. Priebe [54] developed a model based on di-

mensionless form of heat conduction equation but this model did not compute thermal damage and was not experimentally validated. Then a model for the study of thermal effects of Nd:YAG laser on biological tissues was presented by Cummins and Nauenberg [55]. This model differed from Halldorson and Langerholc in its discussion of the effect of modifications of tissue properties but it was validated using thermal data obtained by Halldorson and Langerholc on dog stomach [56]. Motamedi [57] proposed a three step model which calculated the damage depth using the Henriques equation and the results matched those measured in dog stomach when irradiated in vivo with Nd:YAG laser. A new model was developed by Jacques [58] which estimated the steady-state temperature in biological tissue with no damage prediction. Mouse skin treated in vitro was used to validate the model. Many models were developed which studied the effect of Nd:YAG laser on myocardium coagulation, on tissue heating with pulsed Nd:YAG laser considering two-dimensional photon diffusion and heat flow equations and on gastrointestinal tissue using heat conduction equation by Derbyshire [59], Grossweiner [60] and Korolyov [61], respectively. Diaz et al. [62, 63] modeled the thermal damage for the laser irradiated cartilage using heat diffusion equation on the tissue slab using a finite element method. Recently, Zhou et al. [64] used seven-flux model and the bio-heat transfer equation to study thermal damage in laser-irradiated tissue. Many of these models used complex mathematical solutions and some used simple solutions but were not useful for special cases of clinical applications. To date, there is no such model which considers the interface of the tumour inside the tissue and monitors the damage front propagation with respect to the tumour boundary, depending on the exposure time for a particular laser power. In this model the factors which dominantly affect the absorption coefficient like melanosome volume fraction in epidermis, water content and blood volume in dermis.

The objective of this work is to develop a mathematical model to estimate the temperature distribution inside the tissue and depth of thermal damage during the thermal therapy of Basal Cell Carcinoma when irradiated with Continuous Wave (CW) Nd:YAG laser having Gaussian beam profile. In addition to developing such a model, this work also strives to arrive at a quantitative correlation between optimised exposure time and laser power for a particular tumour radius. The finite volume method has been used to solve an axisymmetry bio heat equation for 2-D tissue slab to predict temperature. To estimate the irreversible thermal damage depth, the Arrhenius equation is used. The effect of tissue optical properties and laser parameters on the thermal damage is discussed in this study for different tumour radii.

1.5 Outline of the thesis

Development of a heat transfer model for parametric studies on laser tissue interactions is the main work of this thesis. This thesis consists of three chapters. A brief description of each chapter is given below.

Chapter 1: This chapter consists of general background of historical necessity of study of laser tissue interaction, advancement in medical lasers, application in medical diagnostics and therapeutics, literature review and objective of the study.

Chapter 2: A theoretical model for laser interaction with tissue, based on Beer-Lambert's Law and beam broadening model, is developed in this chapter. Phenomena like absorption of laser energy, scattering of laser energy, photo coagulation (denaturation) of proteins, and subsequent photovaporisation of tissue water content, due to the rise in temperature have been studied. The dominant factors for absorption and scattering in epidermis and dermis are considered along with the laser power, beam radius and wavelength. The Pennes bio heat equation with boundary conditions is solved for the 2-D axisymmetric multilayered tissue model with a carcinoma of specific depth and radial spreading using finite element method to estimate the temperature. The spatial and temporal damage is estimated by using Henriques' theory of skin burns which uses Arrhenius equation. Also, in this chapter the validation of the code developed is done using the experimental results from literature.

Chapter 3: In this chapter, the results obtained from the study are discussed and a correlation is proposed between optimised exposure time and laser power for a particular tumour radius. On the basis of these results, the conclusions are drawn.

Chapter 4: Summary of the whole thesis is in this chapter. The direction of future work has been presented.

CHAPTER 2

Theoretical Background

2.1 Physical description and Model

In this mathematical model, a slab of three-layered biological tissue having a BCC of a particular depth and spreading radius at the surface is irradiated with Gaussian laser beam profile. The tissue surface is assumed to be a perfectly insulated interface and the thermal energy distribution is supposed to be axisymmetric. The bio-heat equation for 2-D three-layer tissue model is solved using finite volume method. The implicit three time level method is used to solve the unsteady part to obtain the second order accuracy in time. When the laser beam is impinged on the tissue surface, the thermal response of a biological tissue is given by Pennes bio-heat equation as below.

$$\rho.c.\frac{\partial T}{\partial t} = k.\nabla^2 T + S - \dot{w}_b \tag{2.1}$$

where ρ is the density of the tissue, T is the temperature, S is the source term, k is the thermal conductivity of tissue, c is the specific heat, $\dot{w}_b$ is the blood perfusion rate.

2.1.1 Source Term

The source term comes into play because of laser-tissue optical interactions like reflection, absorption, and scattering. Many authors have developed mathematical models using different methods like Beer-Lambert's law, seven-flux model, Kubelka-Munk theory, photon diffusion approximation, multiple scattering, and Monte Carlo model [47, 65, 66]. The selection of model relies on the laser parameters like wavelength and

the precision required as well as the optical and thermal properties of the tissue. The laser light experiences scattering, if the wavelength lies in the Infra-red and visible spectrum range, when impinged on the biological tissue. There have been studies on animal skin in vivo [67], canine and human myocardium [68], and liver treated in vitro [69] to confirm the scattering of wavelengths in the range of IR and visible spectrum. The beam broadening model proposed by Yoon et al. [65] considered the scattering phenomenon along with the absorption of light. and beam broadening occurred due to multiple scatterings. The intensity (I) at the point (r,z) can be determined by the relation:

$$\mathrm{I(r,z)} = \mathrm{(1\text{-}R)} \times \mathrm{I_0}.\mathrm{e}^{-0.5.(\mathrm{r}/\tau(\mathrm{z}))^2}.\mathrm{e}^{-\gamma.\mathrm{z}} \tag{2.2}$$

where I(r,z) is the intensity or irradiance, R is the direct reflection coefficient from the tissue surface, γ is the extinction coefficient and is equal to $\mu_a + \mu_s$, where μ_a and μ_s are absorption and scattering coefficients respectively, $\tau(\mathrm{z}) = \tau_0.\mathrm{e}^{(-\mu_s/2).\mathrm{z}}$, $\tau_0$is the standard deviation of beam.

The value of R is dependent on tissue properties and laser wavelength as described by Kikuchi [70] for hepatic tissue. The derivative of equation 2.2 gives the source term S(r,z):

$$\mathrm{S(r,z)} = \mu_a \times \mathrm{I(r,z)} + \mu_s.\left\{1 - 0.5 \times (\mathrm{r}/\tau(\mathrm{r}))^2\right\} \times \mathrm{I(r,z)} \tag{2.3}$$

The values of tissue optical properties considered in the model are based on the news report on the summary of skin optical properties by Steven L. Jacques [71], which discusses the selection of approximate optical coefficients for absorption and reduced scattering of skin with variable amounts of melanin and blood perfusion.

In this study, the tissue optical properties like absorption and scattering coefficient, for different skin layers considered are $\mu_{a.epi} = 571.29cm^{-1}$, $\mu_{a.derm} = 41.24cm^{-1}$, $\mu_{a.subfat} = 10.0cm^{-1}$, $\mu_{s.derm} = 732.31cm^{-1}$ and $\mu_{s.subfat} = 918.58cm^{-1}$.

2.2 Calculation of Optical and Thermal Parameters of Tissue

2.2.1 Epidermis

The total optical absorption coefficient ($\mu_{a.epi}$) of the epidermis is a result of absorption due to minor baseline and absorption due to melanin which depends on the volume

fraction of melanosomes in the epidermis.

Baseline absorption coefficient of melanin less epidermis, $\mu_{a.skinbaseline}$

The absorption coefficient values linked with melanin less epidermis and bloodless dermis are difficult to be differentiated. The baseline absorption of both epidermis and dermis are approximated by the following $\mu_{a.skinbaseline}$, expressed as a function of wavelength (nm):

$$\mu_{a.skinbaseline} = 0.244 + 85.3exp(-(nm-154)/66.2)\,[cm^{-1}] \tag{2.4}$$

The integrating sphere calibrated using phantom measurements was used to carry out quantitative analysis of bloodless rat skin which forms the base for the expression (Ruiping Huang, S. Jacques, unpublished data). The haemoglobin and bilirubin residues in the neonatal skin samples elucidated the excessive absorption in the data generated for an in vitro study conducted for $450-750nm$ by Iyad Saidi [72] using an integrating sphere. The expression for approximating that data is:

$$\mu_{a.skinbaseline} = (7.84\times10^{8})(nm^{(-3.255)})\,[cm^{-1}] \tag{2.5}$$

Absorption coefficient of a single melanosome, $\mu_{a.mel}$

The factor that dominates the absorption in epidermis is melanin concentration. Melanin has a broad absorption spectrum with a property to exhibit strong absorption at shorter wavelengths. Melanin granules, $10nm$ in size, are found in the internal membranes of membranous particles called melanosomes which are of 1-2μm diameter. The magnitude and wavelength dependence (nm) of average absorption coefficient of a melansome, $\mu_{a.mel}$, is estimated by the expression:

$$\mu_{a.mel} = (6.6\times10^{11})(nm^{(-3.33)})\,[cm^{-1}] \tag{2.6}$$

The absorption coefficient value due to melanin at the Nd:YAG laser wavelength ($1064nm$), $\mu_{a.mel} = 55cm^{-1}$.

The various published studies carried out by Jacques and McAuliffe [73] for the threshold exposure for explosive vaporisation of melanosomes by pulsed lasers at various wavelengths forms basis for this expression. The expression estimates only the approximate values of average melanosome absorption coefficient because the melanin contents of melanosomes differ considerably.

Table 2.1: Volume fraction of epidermis occupied by melanosomes for differently pigmented skins.

Skin Type	Volume fraction (f_{mel})
Light-skinned adults	1.3 – 6.3%
Moderately pigmented adults	11 – 16%
Darkly pigmented adults	18 – 43%

Volume fraction of melanosomes in epidermis

The melanin concentration ranges are expressed as the volume fraction of the epidermis occupied by melanosomes (f_{mel})[74]:

The Table2.1 shows the percentage of epidermis volume occupied by the melanosomes. The volume fraction varies from 1.3 – 43%. In this model the volume fraction (f_{mel}) is considered to be 10% which lies in the range for moderately pigmented adults.

Net epidermal absorption coefficient, $\mu_{a.epi}$

The total epidermal absorption coefficient, $\mu_{a.epi}$, results from the combination of the baseline skin absorption and the melanin absorption. It is estimated by:

$$\mu_{a.epi} = (f_{mel})(\mu_{a.mel}) + (1 - f_{mel})(\mu_{a.skinbaseline}) \tag{2.7}$$

Scattering coefficient of the epidermis

In this model, the scattering coefficient of epidermis and dermis are considered separately, since there is a small difference between $\mu_{s.epi}$ and $\mu_{s.derm}$, as discussed in the report of Steven Jacques [71]. As the epidermis is a thin layer so the details of $\mu_{s.epi}$ becomes less important for visible and near-infrared applications involving photon diffusion. The minor differences in $\mu_{s.derm}$ are significant for the techniques and devices whose mechanism of action depends upon photon interaction with epidermis.

Another important tissue parameter which affects the photon distribution inside the biological tissue is its anisotropy (g). The values of g for this model are taken in the range of 0.7 – 0.95 for skin tissue which vary with the wavelength. As laser therapy involves many scattering events so the details of $\mu_{s.epi}$ and g_{epi} become less important than the lumped parameter $\mu_{sp.epi}$, called the reduced scattering coefficient:

$$\mu_{sp.epi} = (\mu_{s.epi})(1 - g_{epi}) \tag{2.8}$$

2.2.2 Dermis

The total optical absorption coefficient of the dermis ($\mu_{a.derm}$) is chiefly a result of haemoglobin absorption due to cutaneous blood perfusion with the contribution of baseline skin absorption being insignificant. The optical effects of the depth of the blood are neglected for an average $\mu_{a.derm}$.

Baseline absorption coefficient of bloodless dermis, $\mu_{a.skinbaseline}$

The absorption due to baseline is almost similar for both dermis and epidermis and thus can be considered as $\mu_{a.skinbaseline}$.

Absorption coefficient of blood, $\mu_{a.blood}$

In dermis, haemoglobin of cutaneous blood accounts for the major part of absorption of laser light which is impinged on the tissue. The value of absorption coefficient of blood for $1064nm$ wavelength is taken from the data of Wray et al.[75]. The data for oxygenated and de-oxygenated blood was generated but in this study, only oxygenated blood is considered. The volume percentage of red blood cells in blood is known as hematocrit value which is 45% for males and is considered for this study. But for females it is 40%.

Absorption coefficient of dermis perfused with blood, $\mu_{a.derm}$

The average volume fraction of blood, f_{blood}, can be specified based on the assumption that the blood is uniformly distributed in the skin. The value of $f_{blood}$for this model is taken as 0.2%. The blood volume fraction is $2-5\%$ in venous plexus which is about $100-200\mu m$ from the surface and this is similar to other well-perfused tissue. For the average homogeneous f_{blood}, the absorption of the dermis, $\mu_{a.derm}$, is expressed as:

$$\mu_{a.derm} = (f_{blood})(\mu_{a.blood}) + (1 - f_{blood})(\mu_{a.skinbaseline}) \tag{2.9}$$

Scattering coefficient of dermis

The scattering due to dermis, called reduced scattering ($\mu_{sp.derm}$), is a combination of Mie scattering by the large cylindrical dermal collagen fibers and the Rayleigh limit scattering by the small-scale structures associated with the collagen fibers and other cellular structures. The scattering coefficient ($\mu_{s.derm}$) and anisotropy (g_{derm}) can be calculated using Mie theory and using these, reduced scattering coefficient ($\mu_{sp.derm}$) can be calculated. The reduced scattering coefficient ($\mu_{sp.epi}$) for epidermis is approximated by

($\mu_{sp.derm}$) because of similar behaviour of epidermis owing to the presence of keratin fibers.

The following relation can be used to simulate the Mie scattering behaviour:

$$\mu_{sp\_Mie.fibers}(nm) = (2 \times 10^5)(nm^{(-1.5)})\,[cm^{-1}] \tag{2.10}$$

The expression for estimation of the Rayleigh scattering component in dermis is:

$$\mu_{sp\_Rayleigh}(nm) = (2 \times 10^{12})(nm^{(-4)})\,[cm^{-1}] \tag{2.11}$$

The total reduced scattering is the combination of the Mie and Rayleigh scattering:

$$\mu_{sp}(nm) = \mu_{sp\_Rayleigh}(nm) + \mu_{sp\_Mie.fibers}(nm) \tag{2.12}$$

The scattering due to small-scale structures follows Rayliegh scattering at short wavelengths below $650nm$ while the scattering from fibers at longer wavelengths above $650nm$ is dominated by Mie scattering.

2.2.3 Subcutaneous Fat

Absorption and Scattering coefficient of Subcutaneous Fat

The absorption coefficient of subcutaneous fat, $\mu_{a.subfat} = 10.0cm^{-1}$ was shown by Simpson et al. [76] using the integrating sphere technique for the range of $620-1000nm$.

The study conducted by the Bashkatov et al. [77] described that for human subcutaneous adipose tissue scattering coefficient, $\mu_{s.subfat}$, for the spectral range from $600-1500nm$, follows the power law and the results matched the experimental findings. The expression that can be used to estimate the $\mu_{s.subfat}$ is called as power law:

$$\mu_{s,subfat}(\lambda) = 1050.6 \times \lambda^{-0.68}\,[cm^{-1}] \tag{2.13}$$

Thermal Parameters of dermis and sub-cutaneous fat

The three important thermal parameters of tissue viz., density (ρ), specific heat (c), and thermal conductivity (k) are influenced by the water content of the tissue, the initial value of which is considered to be 70%[78]. The water starts to evaporate when temperature exceeds 100^oC, because of vaporisation. The model proposed by Dua and Chakraborty [79] described phase change processes, like melting and vaporisation, in

treatments with high irradiance. In photo-thermal therapy, where temperature can exceed the vaporisation temperature of water inside the tissue, photovaporisation can occur and hence the water fraction changes with time. These three key tissue thermal parameters for different water fractions at different time instances of thermal therapy can be described as[80] :

$$\rho\,(kg/m^3) = (6.16 \times 10^{-2} W + 0.938)^{-1} \tag{2.14}$$

$$c\,(J/kg\,K) = 2.5W + 1.7 \tag{2.15}$$

$$k\,(W/m\,K) = \rho \times 10^{-5}(0.454W + 0.174) \tag{2.16}$$

where W is the water mass content.

In this model, thermal parameters are constant and energy distribution is symmetric about the z-axis, so the bio-heat equation is expressed in cylindrical coordinates:

$$\rho.c.\frac{\partial T}{\partial t} = k\left\{\frac{\partial^2 T}{\partial r^2} + \frac{1}{r}.\frac{\partial T}{\partial r} + \frac{\partial^2 T}{\partial z^2}\right\} + S \tag{2.17}$$

This equation 2.17 is solved using finite volume method for 2-D biological tissue slab. There are many other analytical methods to solve this equation but their computational time hinders the determination of the temperature during the transient state. To minimise the computational time, numerical solutions which can approximate the exact solution and determine the transient temperatures in short time, can be used.

The cross-section of 2-dimensional three-layer skin model with the basal cell carcinoma penetrating inside the dermis, on which the laser beam is irradiated, is shown in Figure 2.1.

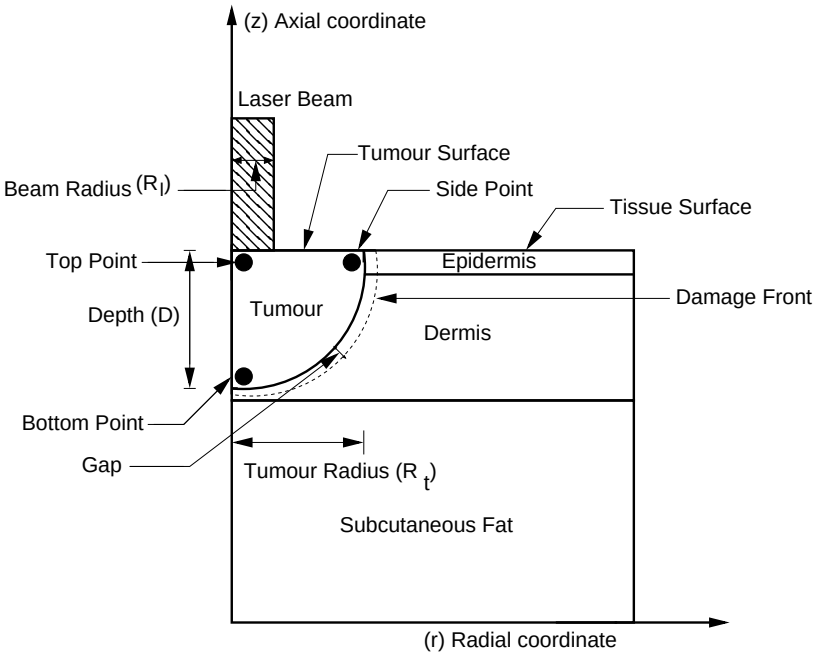

Figure 2.1: Schematic diagram of 2-D three layer skin model.

The depth (D) is taken from the level of normal skin surface. The tumour depth (D) is considered equal to tumour radius (R_t) for this study. The beam radius (R_l) is kept 1.75 times the tumour radius, i.e. Beam Radius (R_l) = 1.75 × Tumour Radius (R_t). The three black dots marked as top point, side point and bottom point are shown for which the temperature is monitored throughout the laser exposure and even after the laser irradiation is terminated. The gap can be defined as the distance between the tumour interface and the thermal damage front. The boundary conditions for this model are:

$$-k.\frac{\partial T}{\partial r} = 0 \text{ at r=0} \qquad -k.\frac{\partial T}{\partial z} = h(T - T_0) \text{ at z} = z_{top} \qquad T = T_0 = 37^oC \text{ at r} = r_{tissue} \text{ and z} = 0$$

Figure 2.2 displays typical 2-D non-uniform grid arrangement. The finer grid is laid from top to bottom near z-axis because the laser is impinged at that point and the temperature gradient is higher at that particular location. In the grid a regular shaped tumour interface is shown whose depth and radius can be varied. The grid density used is 130 × 130.

The table 2.2 shows the series of biological phenomena which occur during the photothermal therapy at different temperatures. For this case, the temperature of the tissue reaches up to 100^oC, so the biological effects considered are bio stimulation, hyperthermia, reduction in enzyme activity, protein denaturation and vaporisation.

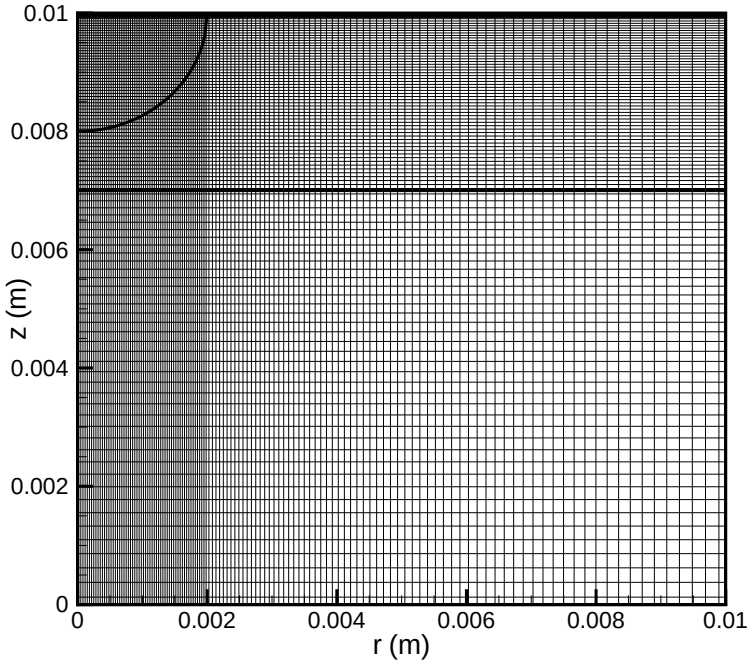

Figure 2.2: A typical 2-D grid arrangement for the model.

Table 2.2: Thermal effect of laser radiation[6].

Temperature (^{o}C)	Biological Effect
37	Normal
< 43	Bio stimulation
$43-45$	Hyperthermia
50	Reduction in enzyme activity
60	Protein denaturation (coagulation)
$70-80$	Welding
80	Permeabilization of cell membranes
100	Vaporization
> 150	Carbonization
> 300	Rapid cutting and ablation

2.3 Thermal Damage Parameter Prediction (Ω)

The potential feature of laser is to heat the target area locally, which in turn can lead to temperature rise. This temperature rise can lead to thermal denaturation of collagen and inactivation of proteins and enzymes which help in the metabolic activity of the tissue. This irreversible thermal coagulation can result in tissue necrosis. The extent of thermal damage in a living tissue, represented by damage parameter (Ω), is defined as:

$$\Omega = ln\left(\frac{C_0}{C_0 - C_d}\right) \tag{2.18}$$

where C_0 is the protein concentration in a normal tissue and C_d is the concentration of denatured protein. The complete tissue necrosis of the basal epidermis layer of the laser irradiated pig skin was indicated by $\Omega = 1.0$ for particular values of rate coefficients considered by Henriques [81]. Welch [82] used $\Omega = 0.53$ as the threshold value above which the thermal damage was considered to be irreversible while the value of $\Omega = 1$ corresponds to denaturation of 63% of the total protein molecules if it is uniform single protein medium. The damage parameter can be estimated using the Arrhenius equation as examined by Henriques [81] after studying the thermal damage in pig skin. The thermal denaturation occurs due to the tissue burns caused by hyperthermia. So, the damage parameter (Ω) is defined as:

$$\Omega(\mathrm{r,z,t}) = \mathrm{A}\int_{\mathrm{t_1}}^{\mathrm{t}_f} exp\left(-\frac{\mathrm{E}_a}{\mathrm{RT}}\right)\mathrm{dt} \tag{2.19}$$

where A is the frequency factor, E_a is the activation energy of denaturation reaction, R is the universal gas constant, 8.314 J/mol.K, T is the absolute temperature of the tissue at the point where Ω is to be calculated, t_1 is the time at the onset of laser exposure, and t_f is the time when the thermal damage is evaluated. There are different values of activation energy and frequency factor given by many authors till date as listed in Table 2.3. The values of frequency factor and activation energy for this study are considered as $A = 3.1 \times 10^{98}$ (1/s) and $E_a = 6.28 \times 10^5$ (KJ/kmol) [81].

2.4 Code validation

The present numerical model is validated by the experimental results of Beacco et al. [51]. They conducted experiment on Wistar rat using CO_2 laser of Biophysics Medical,

Table 2.3: Values of characteristic coefficients of denaturation defined for various injury models.

Injury Model	Temperature Range (^{o}C)	Activation Energy E_a (KJ/kmol)	Frequency Factor A (1/s)
Henriques [81]	All T	6.27×10^5	3.1×10^{98}
Fugitt [83]	T ≤55	6.27×10^5	3.1×10^{98}
	T>55	2.96×10^5	5.0×10^{45}
Stoll and Greene [84]	T≤50	7.82×10^5	2.185×10^{124}
	T>50	3.27×10^5	1.823×10^{51}
Takata [85]	T≤50	4.18×10^5	4.322×10^{64}
	T>50	6.69×10^5	9.389×10^{104}
Wu [86]	T ≤50	6.27×10^5	3.1×10^{98}
	T>50	$6.27 \times 10^5 - 5.10 \times 10^2 \times (T-53)$	3.1×10^{98}
Metha and Wong [87]	All T	4.7×10^5	1.4×10^{72}

France. The rat was exposed to laser beam of power 9 Watts with spot diameter of 5mm for 0.4 second duration. The optical properties of rat liver tissue are $\mu_a = 200cm^{-1}$ and $\mu_s = 0cm^{-1}$. The surface temperature of the tissue during heating was recorded using an infrared camera of AGEMA Thermovision 720 make. The temperature profile measured at the spot center is then compared with the temperature profile generated by the mathematical model so as to validate the accuracy of the model used. It can be observed in Figure 2.3 that our numerical prediction is matching reasonably well with the experimental observation.

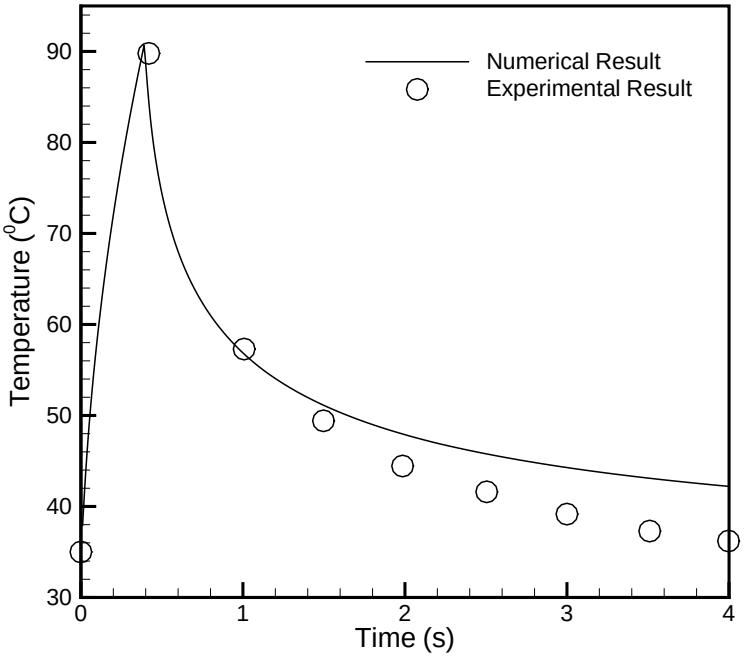

Figure 2.3: Temperature profiles of CO_2 laser. Experimental and numerical results compared.

CHAPTER 3

Results and Discussion

The bio-heat equation is solved using finite volume method for 2-D axisymmetric three-layered skin model with tumour of specific depth starting from the surface of the skin. The tissue optical properties are: $\mu_{a.epi} = 571.29cm^{-1}$, $\mu_{a.derm} = 41.24cm^{-1}$, $\mu_{a.subfat} = 10.0cm^{-1}$, $\mu_{s.derm} = 732.31cm^{-1}$ and $\mu_{s.subfat} = 918.58cm^{-1}$, and the laser parameters for CW Nd:YAG laser are: beam radii =2.625mm, 3.0625mm and 3.5mm for Tumour radii = 1.5mm, 1.75mm and 2.0mm respectively. The average power is varied between $5.0 - 10.0W$. The values of key thermal properties of tissue like density (ρ), specific heat(c), and thermal conductivity (k) depend on the water content which can be calculated using equations 2.14, 2.15, and 2.16 respectively. The initial temperature of the tissue is taken as 37^oC. The laser irradiation time for which the damage front moves 0.2mm beyond the tumour interface into the surrounding healthy tissue is considered to be the optimised irradiation time. This margin is taken into account so as to minimise the recurrence rate. The profiles for gap with respect to angle for different time instances, damage integral for side and bottom point with respect to time, temperature with respect to time for top, side and bottom point, and movement of damage front for different time instances have been plotted for different tumour radii. In the plots where gap is plotted, the profiles are shown for the five time instances: (i) at the half of the irradiation time, (ii) at the time instance when laser is terminated, (iii) at the time instance where the damage front just touches the tumour interface near the $\theta = 0^o$, (iv) at the time instance after which the damage front almost stops to propagate further and, (v) at time instance after which it totally stops further penetration.

3.1 Gap profiles for different laser powers and different tumour radii

In the Figure 3.1, gap profiles for three different tumour radii are shown for laser power of 9W. The positive value of gap shows that thermal damage front is still inside the tumorous tissue and if the gap value is negative it implies that the thermal damage front has crossed the tumorous tissue and reached the surrounding healthy tissue. The irradiation time for all the cases is different because of different tumour sizes and it is noticed that the damage front for every case moves a certain distance away from the interface into the healthy tissue. The necrosis of any tumorous tissue, if any, in that particular margin is ensured by allowing the damage front to propagate approximately up to $0.4mm$ away from the interface to minimise the recurrence rate. Another interesting observation that can be made is that the damage front for tumour radius $1.5mm$ propagates non-uniformly, i.e., till $\theta = 40^o$ it is uniform then decreases suddenly till $\theta = 70^o$ and then becomes uniform till $\theta = 90^o$, as compared to the propagation of damage front in other two cases as shown in Figure 3.1(a), Figure 3.1(b) and Figure 3.1(c). The damage front for all the three tumour radii almost stops proceeding after a particular time instance like $3s$, $5s$, and $8s$ for tumour radii $1.5mm$, $1.75mm$, and $2.0mm$ respectively.

The Figure 3.2(a), shows the gap profile for tumour radius $1.5mm$ in which it can be noticed that near $\theta = 80^o$ is almost near the interface and the margin is very less for this particular irradiation time, but increasing the irradiation time by $0.1s$ increases the damage of healthy tissue goes above $0.5mm$ which is undesirable. Another observation that can be made is that the damage front just after the $0.05s$ of the laser termination does not cross the interface for $1.5mm$ tumour radius whereas for $1.75mm$ tumour radius it crosses the interface and for $2.0mm$ tumour radius the damage front crosses the interface at the time of laser termination at an angle above $\theta = 20^o$. This can be explained as the distribution of temperature for $1.5mm$ radius is uneven because of the effect of small beam radius so the energy propagation is more in axial direction as compared to radial direction. For the smaller tumour radius, the penetration rate is faster as compared to higher tumour radius as shown in Figure 3.2. Also, it can be noticed that as the power is reduced, the optimum irradiation time increases for a particular tumour radius due to the fact that energy per unit area per unit time decreases for the lower laser powers. These plots depict that the damage front initially moves faster in the radial direction but as the time progresses and the laser exposure is terminated, the damage front penetrates more in axial direction compared to the radial direction as can be seen for the curve at the 15^{th} second. This is because during the laser exposure the temperature gradient is high, and due to scattering coefficient of tissue, the temperature rise is more at the sides than along the axis. But as the laser is turned off, the temperature gradient lowers down speedily at side points because of two reasons: 1) heat diffusion into surrounding tis-

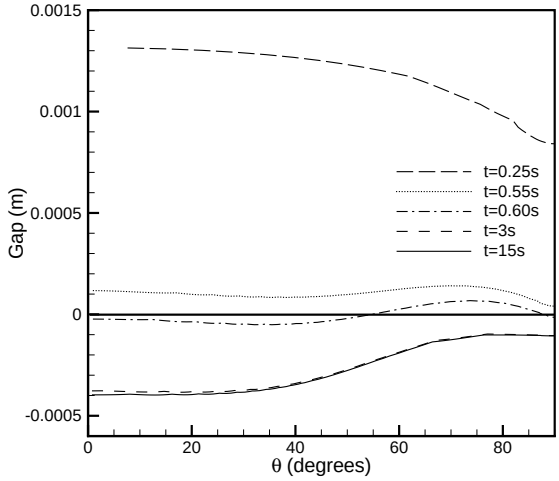

(a) Tumour radius = 1.5mm & Irradiation time = 0.55s

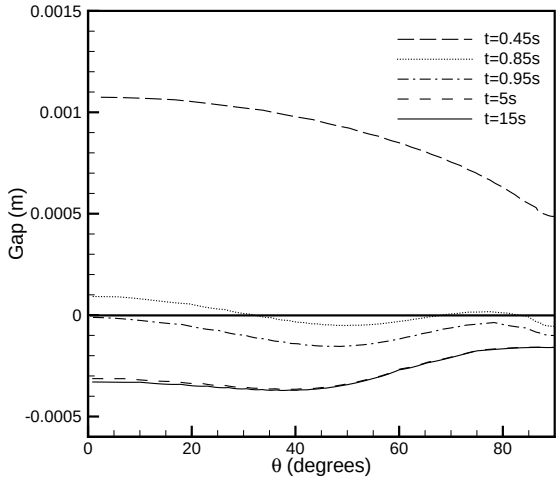

(b) Tumour radius = 1.75mm & Irradiation time = 0.85s

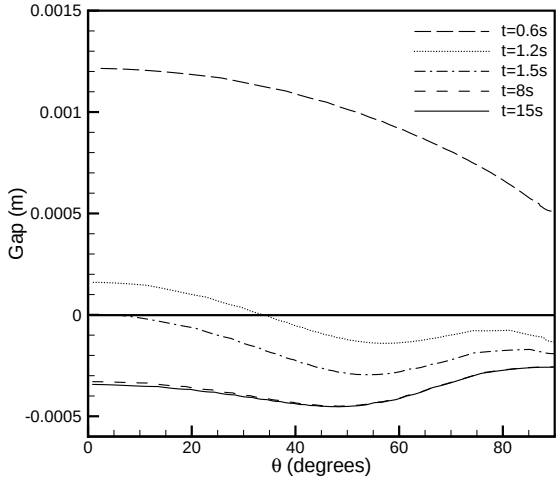

(c) Tumour radius = 2.0mm & Irradiation time = 1.2s

Figure 3.1: Gap profiles for average Laser Power = 9W

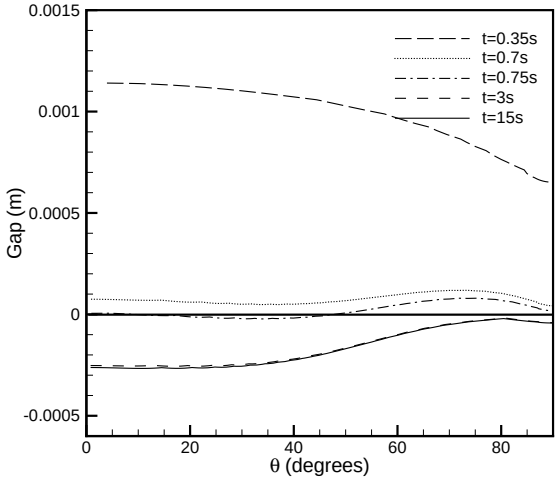

(a) Tumour radius = 1.5mm & Irradiation time = 0.7s

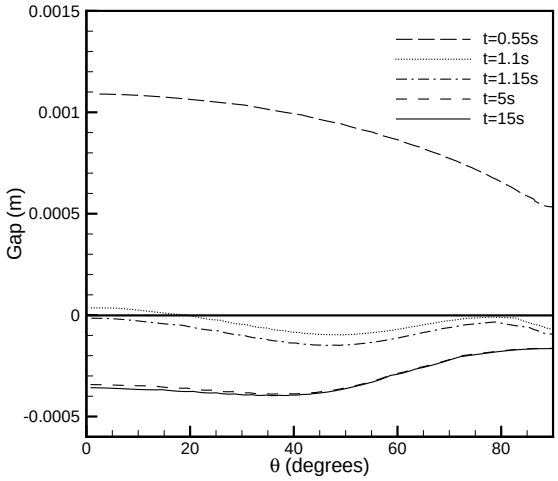

(b) Tumour radius = 1.75mm & Irradiation time = 1.1s

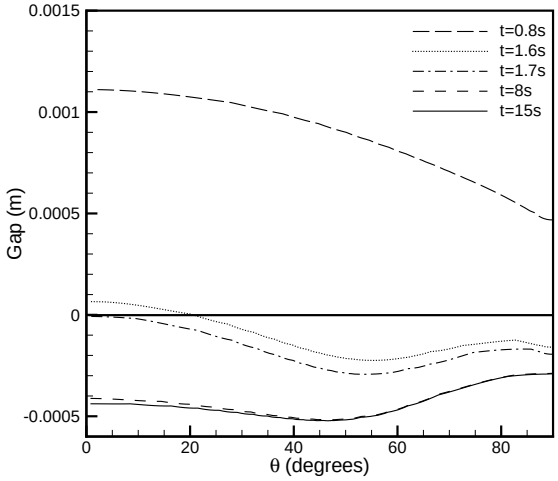

(c) Tumour radius = 2.0mm & Irradiation time = 1.6s

Figure 3.2: Gap profiles for average Laser Power = 7W

sue and 2) dissipation into the air through surface. The temperature gradient decreases slowly for the point at the bottom or away from the surface, since only the diffusion to the surrounding tissue plays a role in lowering the temperature.

In the profile obtained for $1.5mm$ tumour radius for $5W$ power the damage front touches the interface after $1s$ of laser exposure which is the optimum irradiation time for this case as shown in Figure 3.3(a). In Figure 3.3(b), the tumour radius is $1.75mm$ and optimum irradiation time is $1.6s$, but the damage front crosses the interface after $1.5s$ of the laser irradiation which is not the optimum irradiation time. For the case of $2.0mm$ tumour radius, it can be seen that the damage front intercepts the tumour interface at $2.1s$, which is the optimum duration for which laser is impinged on the tissue so as to achieve efficient necrosis of the tumorous tissue and of the healthy tissue up to a particular depth. It is also worth noticing that the rate of penetration is higher during the laser exposure and it decreases drastically once the laser exposure is terminated, as can be seen in all of the above figures.

3.2 Profiles of Damage Integral, (Ω), at bottom and side points near the tumour interface

In the Figure 3.4, the damage integral, Ω, for the bottom and side points for different tumour radii and $9W$ average laser power with respect to time is plotted. The damage integral at side the point is much higher as compared to the damage integral at the bottom point for all three tumour radii. The total damage is recorded as 1750 for the highest tumour radius, 350 for the $1.75mm$ tumour radius and 100 for $1.5mm$ tumour radius. This is because total energy absorbed by the tissue increases with increase in the tumour radius. But, on the other hand, the initiation of noticeable tissue damage represented mathematically by damage integral Ω, is earlier for a tumour with smaller radius. And, this initiation point increases with increase in the tumour radius, e.g. the initiation time for noticeable tissue damage is $0.5s$, $0.75s$ and $1s$ for corresponding tumour radius of $1.5mm$, $1.75mm$, and $2.0mm$ which is because of the fact that the fluence, i.e. energy per unit area per unit time is higher for the lower tumour radius and lower for higher tumour radius. But, the point at the bottom of the tumour near the periphery shows an opposite trend. The total damage at bottom point for $1.5mm$ tumour radius went up to 60, for tumour radius $1.75mm$ it went up to 14 and for $2.0mm$ tumour radius it went the least, i.e. 10. Another interesting trend that can be seen is that the damage front reached the bottom point first for the smallest tumour radius whereas it took increasingly more time for $1.75mm$ and $2.0mm$ tumour radii. This is because the energy per unit area per unit time is highest for the case of $1.5mm$ tumour radius and decreases with an increase in tumour size as indicated in Figure 3.4(b).

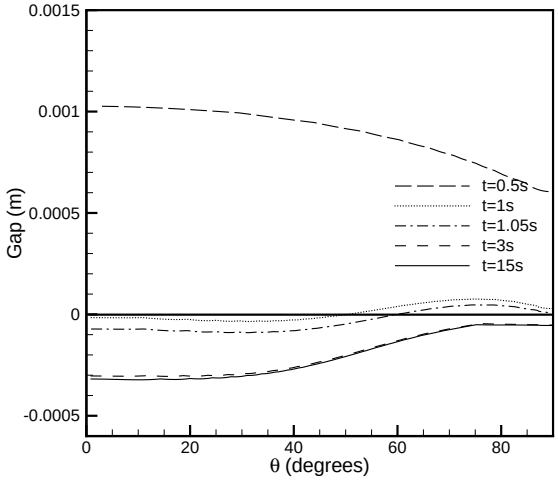

(a) Tumour radius = 1.5mm & Irradiation time = 1.0s

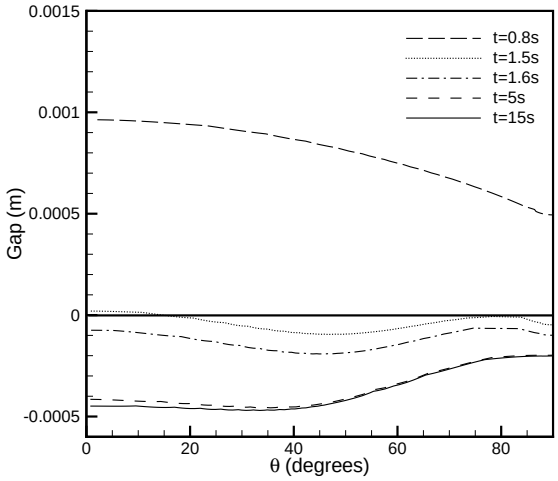

(b) Tumour radius = 1.75mm & Irradiation time = 1.6s

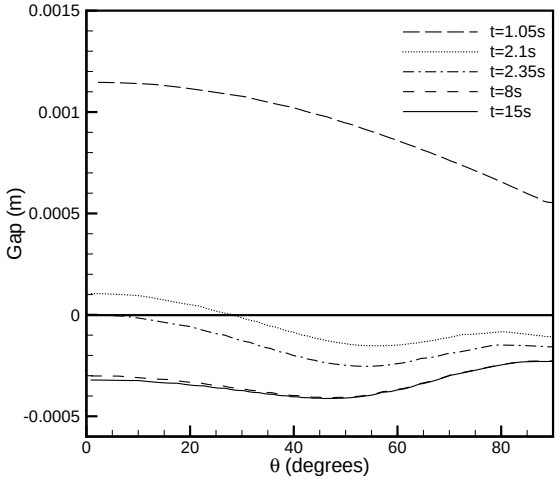

(c) Tumour radius = 2.0mm & Irradiation time = 2.1s

Figure 3.3: Gap profiles for average Laser Power = 5W

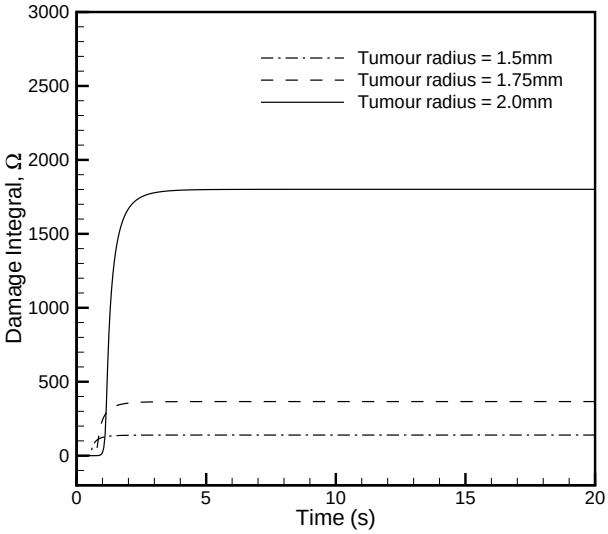

(a) Damage Integral, Ω, at Side point

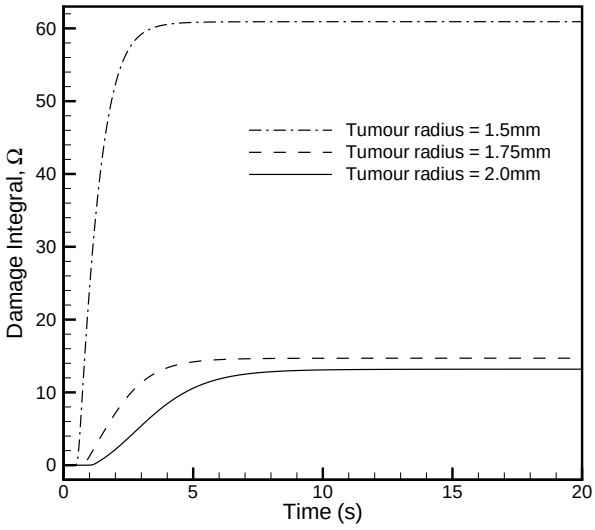

(b) Damage Integral, Ω, at Bottom point

Figure 3.4: Damage Integral profiles for average Laser Power = 9W

Depicted in Figure 3.5 are the integral profiles at side and bottom point of different radii tumour when the average power of the laser used is kept $7W$. It can be noticed that the value of damage integral at side point for $2.0mm$ tumour radius is around 2750, for $1.75mm$ tumour radius it is very low (approximately 300) whereas for $1.5mm$ tumour radius it is just 30. It is becuase the duration for which the laser is impinged for the complete necrosis of the tumour is higher for higher tumour size. Moreover, it can be observed that for larger tumour, the time taken for the temperature to rise above a particular threshold at side point is higher. This results in a late initiation of damage at that point. Similarly trend can also be noticed for laser power of $9W$. The damage integral value for tumour radius of $2.0mm$, $1.75mm$ and $1.5mm$ is 27, 19 and 12 respectively. Also, it can be noticed from the plot that damage integral value reached its maximum at a faster rate for lowest tumour radius, which is $1.5mm$, and as the tumour radius increases the rate of increase of damage integral value decreases as illustrated in Figure 3.5(b). The start of damage at side point of tumour for tumour radius $2.0mm$ when impinged with laser of $7W$ power is $1.5s$ and it started slightly later for the bottom point as can be seen in Figure 3.5(a) and Figure 3.5(b). It can be inferred that the temperature diffusion in axial and radial direction is affected by the optical properties of the skin tissue.

Figure 3.6 illustrates the damage integral profile when the laser of power $5W$ is impinged upon the tumours of different radii. The first point worth noticing is that the maximum value of damage integral at side point in this case went highest for tumour radius $1.75mm$ which is 500, unlike the other cases discussed before. The value of damage integral for tumour radius $2.0mm$ is noticed slightly lower at 450 and the least value is for $1.5mm$ tumour radius. The initiation point for damage in this case moved to $1.75s$ for $2.0mm$ tumour radius. The Figure 3.6(b) depicts the damage integral value profile at bottom point for $5W$ laser power. It can be noticed that the maximum damage value is 44 for the case of $1.75mm$ tumour radius, 24 for $1.5mm$ tumour radius and the least is noticed for $2.0mm$ radius which is 10. The rate of increase of damage integral value is highest for $1.75mm$ radius and it is lowest for $2.0mm$ tumour radius, as shown in Figure 3.6(b). The damage at bottom point of tumour started after $2s$ of the laser exposure for $2.0mm$ tumour radius when impinged with $5W$ laser power.

3.3 Temperature profiles with respect to time at top, side and bottom points near the tumour interface

The variation of temperature with respect to time at three different locations, viz. top, side and bottom, for three different tumour radii is depicted in figure 3.7. The laser power for this case is $9W$. At the point of interaction, temperature went up to 100^oC and

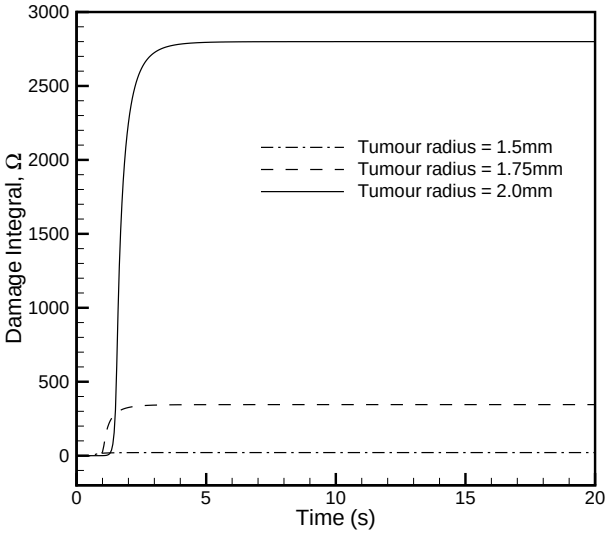

(a) Damage Integral, Ω, at Side point

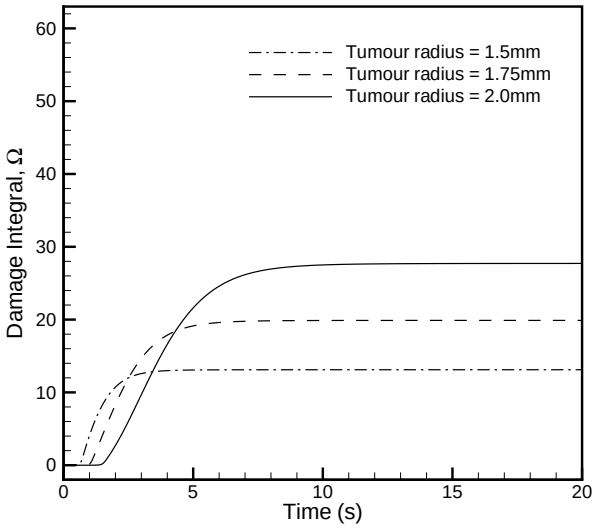

(b) Damage Integral, Ω, at Bottom point

Figure 3.5: Damage Integral profiles for average Laser Power = 7W

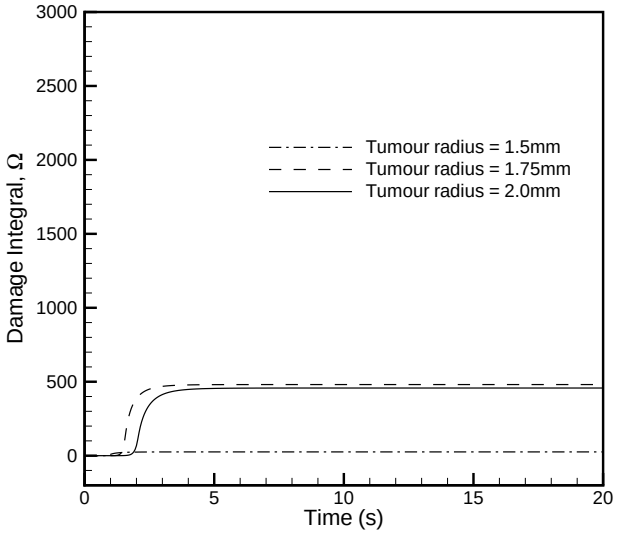

(a) Damage Integral, Ω, at Side point

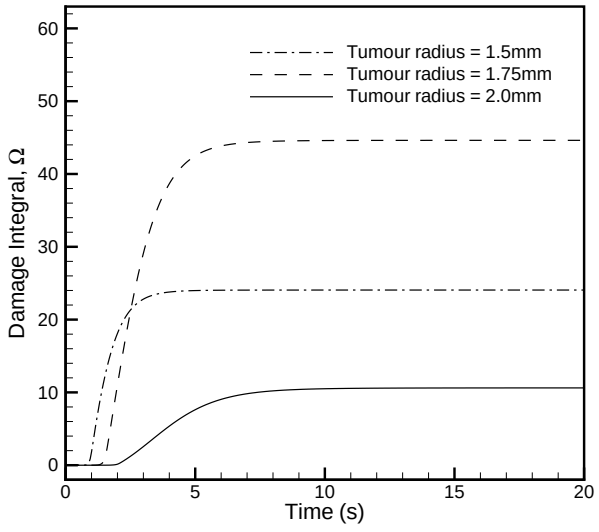

(b) Damage Integral, Ω, at Bottom point

Figure 3.6: Damage Integral profiles for average Laser Power = 5W

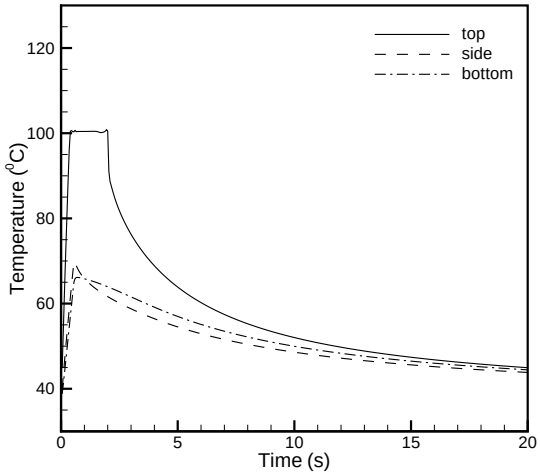

(a) Tumour radius = 1.5mm

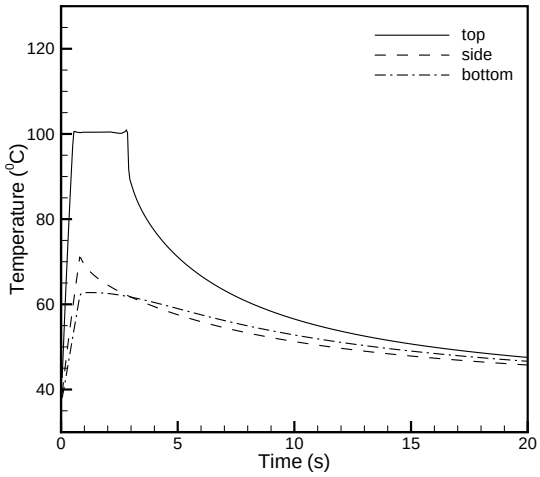

(b) Tumour radius = 1.75mm

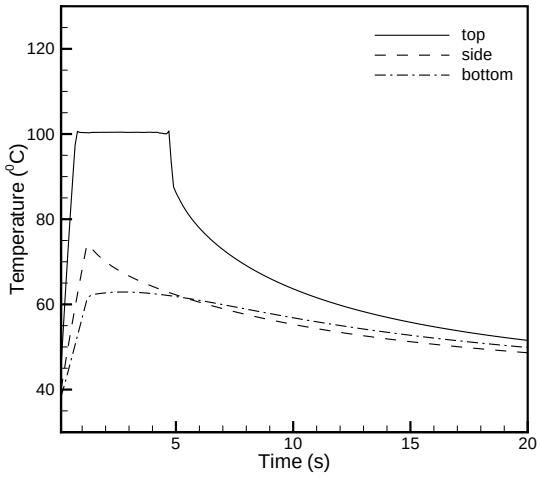

(c) Tumour radius = 2.0mm

Figure 3.7: Temperature profiles for average Laser Power = 9W

then it remained constant for some time, as the water inside the tissue started to vaporise and the temperature dropped drastically when the laser exposure is terminated. This is happening because the heat conduction into the tissue and heat lost into the air are counterbalanced by the heat supplied by the laser source. Once the laser exposure is terminated the heat diffusion into the tissue and the heat dissipation into the air through surface result in the drastic decrease in the surface temperature. As the time progresses, after the laser termination, the temperature decreases at a slower rate because with the passage of time temperature gradient at the surface of the tissue decreases. As a consequence, the rate of heat diffusion decreases. The side and bottom points being at some distance from the point of interaction of laser beam with the tissue, the value of maximum temperature is around 70^oC and 65^oC for side and bottom points respectively. The temperature reduction after the termination of laser exposure is rapid for side point as compared to bottom point. The reason for this is that, side point is close to the surface therefore, heat transfer will be governed by two phenomena: heat diffusion to surrounding tissue and heat dissipation to air. However, for the bottom point only one phenomenon, i.e. heat diffusion to the surrounding tissues, accounts for the heat loss, which is why the temperature decreases at a faster rate for side point as compared to the rate of temperature decrease for the bottom point. In Figure 3.7(b), it can be seen that the temperature profile stays at 100^oC for a longer duration as compared to Figure 3.7(a). This stay is even longer in the profile of temperature plotted for $2.0mm$ tumour radius as shown in Figure 3.7(c). This is because of the larger irradiation time taken to achieve complete necrosis of the tumorous tissue with the increase in tumour radius. Furthermore, owing to the presence of unvaporised water in the tissue, there is no drastic rise in temperature. It can also be observed from these plots that the difference in the maximum temperatures achieved for side and bottom point is low for tumour radius of $1.5mm$, and as the tumour radius increases, the maximum temperature difference between these two points also increases. This is due to higher scattering coefficient of tissue as compared to absorption coefficient and laser irradiation time with the decrease in tumour radius.

The temperature variations for the laser power of $7W$ are shown in Figure 3.8. In these plots it can be noticed that maximum temperature for the side point and bottom point for a tumour radius of $1.5mm$ is 68^oC and 65^oC; it is 73^oC and 65^oC for a tumour radius of $1.75mm$ and 73^oC and 60^oC for a tumour radius of $2.0mm$ respectively. The difference between the maximum temperature at the two points is increasing because of the increase in size of tumour due to which, for a particular duration, temperature diffusion is more in radial direction as compared to axial direction since the scattering coefficient of the tissue is high.

Depicted in the Figure 3.9, are the profiles of temperature for $5W$ laser power for different tumour radii. The maximum temperature for tumour radius of $1.5mm$ at side

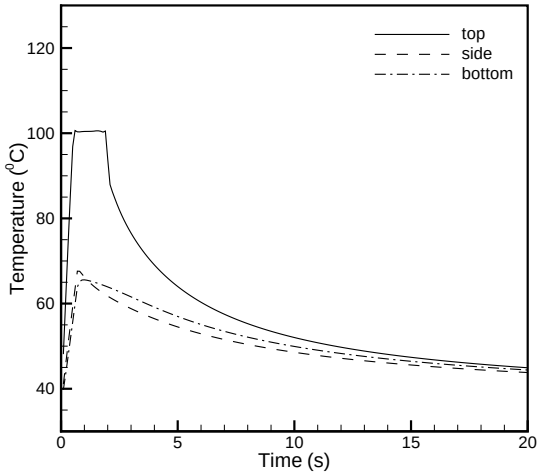

(a) Tumour radius = 1.5mm

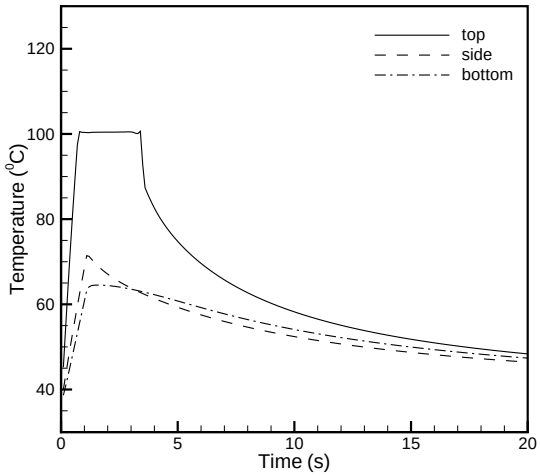

(b) Tumour radius = 1.75mm

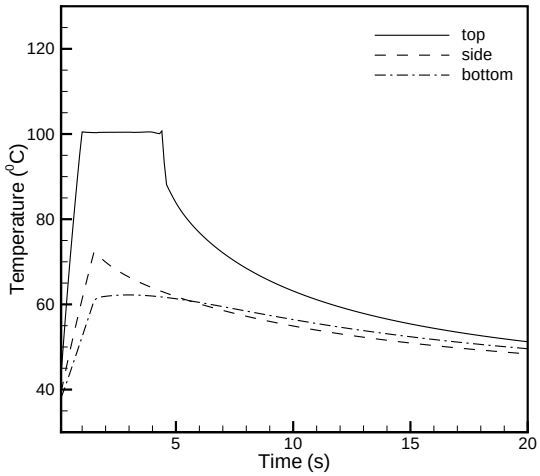

(c) Tumour radius = 2.0mm

Figure 3.8: Temperature profiles for average Laser Power = 7W

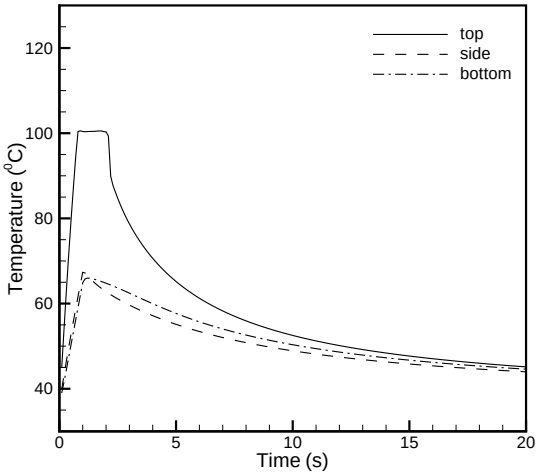

(a) Tumour radius = 1.5mm

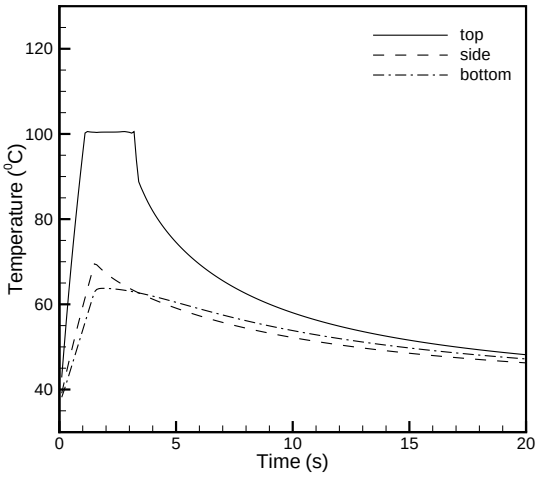

(b) Tumour radius = 1.75mm

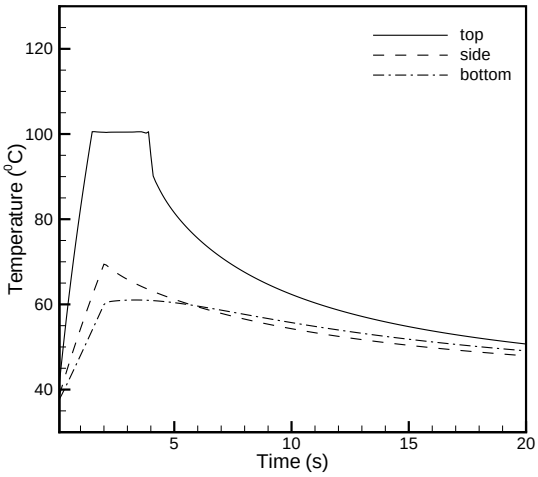

(c) Tumour radius = 2.0mm

Figure 3.9: Temperature profiles for average Laser Power = 5W

Table 3.1: Duration for which the temperature at top point stays above 100^oC.

Power (W)	Tumour Radius $1.5mm$		$1.75mm$		$2.0mm$	
	onset (s)	duration (s)	onset (s)	duration (s)	onset (s)	duration (s)
5	0.80	0.95	1.10	2.35	1.5	2.60
6	0.65	1.50	0.90	1.60	1.2	3.20
7	0.55	1.0	0.75	2.20	1.0	3.85
8	0.45	1.85	0.65	1.70	0.85	3.90
9	0.40	1.60	0.55	2.30	0.75	3.50
10	0.35	1.70	0.50	3.20	0.65	2.65

and bottom points is almost same and is equal to 66^oC. The maximum temperature achieved for these two points for $1.75mm$ tumour radius is 70^oC and 64^oC respectively; for tumour radius $2.0mm$, it is 70^oC and 60^oC respectively. Also, it is illustrated in these profiles that the rate of temperature rise for all the three points decreases as the tumour radius is increased for a particular power because energy per unit area per unit time decreases.

3.4 Onset time instance at which the temperature reaches above 100^oC at top point of tumour interface.

The table 3.1 here shows the onset time instances and the duration for which the temperature rises and stays above 100^oC. In this it can be observed that the onset time instance decreases with the increase in laser power for all the three tumour radii.

3.5 Maximum temperature attained at side and bottom points of tumour.

The maximum temperature achieved at the side and bottom points of the tumour can be seen in the table 3.2 where it can be observed that the difference between the T_{max} of side point and T_{max} of bottom point increases with the increase in tumour radius. Also, the maximum temperature increases with the tumour radius at these two points in general.

Table 3.2: Maximum temperature, T_{max}, at side and bottom points

Power (W)	Tumour radius 1.5mm		1.75mm		2.0mm	
	Side point, (T_{max}) (^oC)	Bottom point, (T_{max}) (^oC)	Side point, (T_{max}) (^oC)	Bottom point, (T_{max}) (^oC)	Side point, (T_{max}) (^oC)	Bottom point, (T_{max}) (^oC)
5	66.67	63.96	70.97	64.67	70.53	61.33
6	69.29	66.85	68.33	61.67	72.07	62.22
7	66.62	63.74	70.73	63.28	73.79	63.04
8	70.88	67.56	68.90	61.33	73.99	62.92
9	69.81	66.14	71.04	62.76	73.30	61.86
10	70.44	66.46	73.71	65.60	70.99	59.86

Table 3.3: optimised exposure duration for lasers of different average powers for various tumour radii

Tumour Radius (mm)	Average Power (Watts)					
	5	6	7	8	9	10
1.5	1.0	0.90	0.70	0.65	0.55	0.50
1.75	1.60	1.20	1.10	0.90	0.85	0.80
2.0	2.10	1.80	1.60	1.40	1.20	1.0

3.6 Correlation between optimised exposure time and laser power for a particular tumour radius.

The laser irradiation time for which efficient tumour necrosis is obtained using laser powers between $5.0W - 10.0W$ for three different tumour radii is listed in table 3.3. The laser powers are taken at a step size of 1.0 for this study. It can be noticed that as the laser power increases for a given radius, the irradiation time decreases almost linearly.

The Figure 3.10 depicts the correlation between the optimised irradiation time and laser power. The symbols show the optimised irradiation time estimated using numerical model and the lines indicate the optimised irradiation time using correlation. It can be clearly seen that the symbols and lines almost fits with each other. The goodness of curve fit is calculated as 97.623% for $5.0-10.0W$ range of laser power and tumour radius lying in between the range of $1.5-2.0mm$. The proposed correlation between irradiation time and laser power for a particular tumour radius is:

$$t_{Irradiation} = (A + B \times P + C \times R_t + D \times P^2 \times R_t^2 + E \times P^3 \times R_t^3) \tag{3.1}$$

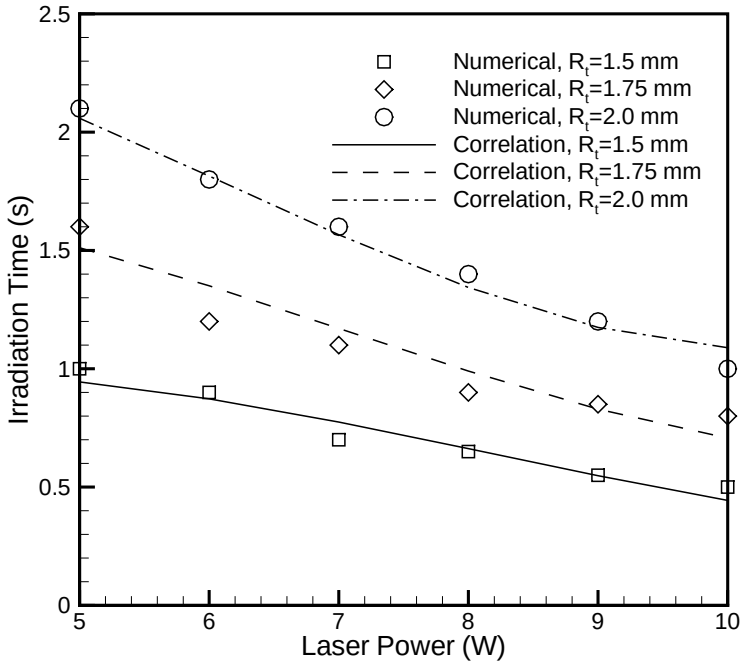

Figure 3.10: Correlation between Irradiation time and Laser Power

where $A = -4.724$, $B = 0.291$, $C = 3.469$, $D = -2.213 \times 10^{-2}$, $E = 6.018 \times 10^{-4}$, $P = laser\ power$, $R_t = tumour\ radius$, $t_{Irradaiation} = irradiation\ time$.

3.7 Conclusion

Models cannot replace the experimental results but simply fortify the experimental outputs and narrow down the range of parameters to be optimised thus resulting in saving the resources and time. A mathematical model that predicts the temperature and monitors the propagation of thermal damage front during the thermal therapy for a particular tissue optical parameters and specific laser parameters is developed. This model reflects the understanding of thermal events like coagulation and vaporisation when the laser of a specific power is impinged on a tumorous tissue. In this study the optimised irradiation time is predicted for a particular tumour radius, laser beam radius, laser power and specific skin type. It can be concluded from the results that irradiation time decreases almost linearly with increase in the laser power for a given tumour radius. The laser beam radius also affects the damage extent and the beam radius has to be optimised for a particular tumour radius so that damage front propagates uniformly. This model cannot be treated as a perfect simulation and the knowledge gained during its development

can be used in future studies. This study also proposes a correlation between optimised exposure time and laser power for a particular tumour radius.

CHAPTER 4

Summary

This study mainly comprises of three sections — (i) Model development and theoretical studies for laser-tissue interactions, (ii) Studying the heat transfer and propagation of damage front inside the tumourous tissue and surrounding healthy tissue for specific laser power and skin type and (iii) Determining optimised irradiation time for different radii of tumour when impinged with laser of particular power and developing a correlation between optimised exposure time and laser power for a particular tumour radius with specific tissue optical and thermal properties. The main objective of this work is to develop a heat transfer model for laser interaction with tissue which can predict optimised irradiation time for efficient necrosis of tumour of particular radius.

The novelty of this developed model for laser interaction with tissue from the existing thermal models for laser tissue interaction is the addition of tumour interface in the grid, which can be varied to simulate different sizes of carcinoma as per the requirement. Also, the model developed, considers different dominant factors responsible for absorption and scattering of light in different layers of the skin. This study quantitatively concludes, that laser power and irradiation time are inversely proportional, for a particular tumour radius.

4.1 Limitations and Recommendations

The model developed does not consider the biological effects like carbonisation and ablation as the temperature achieved, with the parameters considered, is $\leq 100^{o}C$.

The correlation developed is valid for the tumour size between $1.5mm - 2.0mm$ and laser power in the range of $5.0W - 10.0W$. Also, to make the model more realistic, the

absorption in dermis due to blood perfusion can further be divided into oxygenated blood perfusion and de-oxygenated blood perfusion.

The wavelength considered here is $1064nm$ only, but the model can be developed for the wavelength ranging between $600nm - 1100nm$, also known as optical window in medical science.

Bibliography

[1] "Skin-layers-diagram", http://health-advisors.org/skin-layers-diagram/, accessed on 29-05-2013; 12:05 p.m.

[2] M. Gorjan, "Modelling and Measurements of Laser-Skin Thermal Interaction", http://www-f9.ijs.si/textasciitildekrizan/sola/sempod/0708/gorjan.pdf, 2008.

[3] G. J. Muller, B. Chance, and R. Alfano, *Medical optical tomography: functional imaging and monitoring*, SPIE Press, Bellingham, WA, 1993.

[4] J. L. Boulnois, "Photophysical processes in recent medical laser developments: a review", *Lasers in Medical Science*, vol. 1, no. 1, pp. 47–66, 1986.

[5] M. H. Niemz, *Laser-tissue interactions: fundamentals and applications*, (third enlarged edition) ed., Springer-Verlag Berlin Heidelberg, 2004.

[6] L. J. Miserendino, G. C. Levy, and I. M. Rizoiu, "Effects of Nd:YAG laser on the permeability of root canal wall dentin", *Journal of Endodontics*, vol. 21, no. 2, pp. 83–87, 1995.

[7] M. Molls, "Hyperthermia–the actual role in radiation oncology and future prospects. part i", *Strahlentherapie und Onkologie: Organ der Deutschen Rontgengesellschaft ... [et al]*, vol. 168, no. 4, pp. 183–190, 1992.

[8] K. H. Luk, R. M. Hulse, and T. L. Phillips, "Hyperthermia in cancer therapy", *Western Journal of Medicine*, vol. 132, no. 3, pp. 179–185, 1980.

[9] R. A. Steeves, "Hyperthermia in cancer therapy: where are we today and where are we going?", *Bulletin of the New York Academy of Medicine*, vol. 68, no. 2, pp. 341–350, 1992.

[10] T. H. Maiman, "Optical and microwave-optical experiments in ruby", *Physical Review Letters*, vol. 4, no. 11, pp. 564–566, 1960.

[11] M. M. Zaret, G. M. Breinin, H. Schmidt, H. Ripps, I. M. Siegel, and L. R. Solon, "Ocular lesions produced by an optical maser (laser)", *Science (New York, N.Y.)*, vol. 134, no. 3489, pp. 1525–1526, 1961.

[12] C. J. Campbell, M. C. Rittler, and C. J. Koester, "The optical maser as a retinal coagulator: an evaluation", *Transactions - American Academy of Ophthalmology and Otolaryngology. American Academy of Ophthalmology and Otolaryngology*, vol. 67, pp. 58–67, 1963.

[13] H. C. Zweng, M. Flocks, N. S. Kapany, N. Silbertrust, and N. A. Peppers, "Experimental Laser Photocoagulation", *American journal of ophthalmology*, vol. 58, pp. 353–362, 1964.

[14] L. Goldman, P. Hornby, R. Meyer, and B. Goldman, "Impact of the laser on dental caries", *Nature*, vol. 203, no. 4943, pp. 417–417, 1964.

[15] R. H. Stern and R. F. Sognnaes, "Laser beam effect on dental hard tissues", *J. Dent. Res.*, vol. 43, no. 5, p. 873, 1964.

[16] J. Serup, B. E. Jemec, and G. G. L. Grove, *Handbook of non-invasive methods and the skin*, CRC/Taylor & Francis, 2006.

[17] M. H. Niemz, *Laser-tissue interactions: fundamentals and applications*, Springer-Verlag, 1996.

[18] A. J. Welch and J. C. van Gemert Martin, *Optical-thermal response of laser-irradiated tissue*, (second edition) ed., Plenum Press, 1995.

[19] G. H. Jacobs, J. J. Rippey, and M. Altini, "Prediction of aggressive behavior in basal cell carcinoma", *Cancer*, vol. 49, no. 3, pp. 533–537, 1982.

[20] D. L. Miller and M. A. Weinstock, "Nonmelanoma skin cancer in the united states: incidence", *Journal of the American Academy of Dermatology*, vol. 30, no. 5 Pt 1, pp. 774–778, 1994.

[21] G. W. Jung, A. I. Metelitsa, D. C. Dover, and T. G. Salopek, "Trends in incidence of nonmelanoma skin cancers in alberta, canada, 1988-2007", *The British journal of dermatology*, vol. 163, no. 1, pp. 146–154, 2010.

[22] D. Weedon and G. Strutton, *Skin Pathology*, Edinburg:Churchill Livingstone, 2002, 765–772.

[23] M. T. Bastiaens, J. J. Hoefnagel, J. A. Bruijn, R. G. Westendorp, B. J. Vermeer, and J. N. Bouwes Bavinck, "Differences in age, site distribution, and sex between nodular and superficial basal cell carcinoma indicate different types of tumors", *The Journal of investigative dermatology*, vol. 110, no. 6, pp. 880–884, 1998.

[24] M. Nakayama, K. Tabuchi, Y. Nakamura, and A. Hara, "Basal cell carcinoma of the head and neck", *Journal of Skin Cancer*, vol. 2011, pp. 1–9, 2011.

[25] G. M. Menkar and D. S. Chiu, *Basal Cell Carcinoma*, BC Decker, Hamilton, Ga, USA, 2001.

[26] J. Parrish and T. F. Deutsch, "Laser photomedicine", *IEEE Journal of Quantum Electronics*, vol. 20, no. 12, pp. 1386–1396, 1984.

[27] R. Srinivasan and V. Mayne-Banton, "Self-developing photoetching of poly(ethylene terephthalate) films by far-ultraviolet excimer laser radiation", *Applied Physics Letters*, vol. 41, no. 6, pp. 576–578, 1982.

[28] M. H. Niemz, E. G. Klancnik, and J. F. Bille, "Plasma-mediated ablation of corneal tissue at 1053 nm using a Nd:YLF oscillator/regenerative amplifier laser", *Lasers in surgery and medicine*, vol. 11, no. 5, pp. 426–431, 1991.

[29] M. M. Krasnov, "Laser puncture of the anterior chamber angle in glaucoma (a preliminary report)", *Vestnik oftalmologii*, vol. 3, pp. 27–31, 1972.

[30] D. Aron-Rosa, J. J. Aron, M. Griesemann, and R. Thyzel, "Use of the neodymium-YAG laser to open the posterior capsule after lens implant surgery: a preliminary report", *Journal - American Intra-Ocular Implant Society*, vol. 6, no. 4, pp. 352–354, 1980.

[31] F. Fankhauser, P. Roussel, J. Steffen, E. Zypen, and A. Chrenkova, "Clinical studies on the efficiency of high power laser radiation upon some structures of the anterior segment of the eye", *International Ophthalmology*, vol. 3, no. 3, pp. 129–139, 1981.

[32] C. E. Lindholm, E. Kjellen, P. Nilsson, and S. Hertzman, "Microwave-induced hyperthermia and radiotherapy in human superficial tumours: clinical results with a comparative study of combined treatment versus radiotherapy alone", *International journal of hyperthermia: the official journal of European Society for Hyperthermic Oncology, North American Hyperthermia Group*, vol. 3, no. 5, pp. 393–411, 1987.

[33] F. K. Storm, L. R. Kaiser, J. E. Goodnight, W. H. Harrison, R. S. Elliott, A. S. Gomes, and D. L. Morton, "Thermochemotherapy for melanoma metastases in liver.", *Cancer*, vol. 49, no. 6, pp. 1243–1248, 1982.

[34] Prezi, *Modelling and measurements of laser-skin thermal interaction*, 2010.

[35] Z. Amin, J. J. Donald, A. Masters, R. Kant, W. R. Lees, and S. G. Bown, "Interstitial laser photocoagulation therapy for liver tumors: clinical results", pp. 202–209, 1993.

[36] R. Anderson and J. Parrish, "Selective photothermolysis: precise microsurgery by selective absorption of pulsed radiation", *Science*, vol. 220, no. 4596, pp. 524–527, 1983.

[37] F. Manns, P. J. Milne, X. Gonzalez-Cirre, D. B. Denham, J. M. Parel, and D. S. Robinson, "In situ temperature measurements with thermocouple probes during laser interstitial thermotherapy (LITT): quantification and correction of a measurement artifact", *Lasers in surgery and medicine*, vol. 23, no. 2, pp. 94–103, 1998.

[38] K. Yamada, T. Someva, S. Shimada, H. Nakagawa, A. Kukita, H. Tokita, and N. Tanaka, "Thermochemotherapy for malignant melanoma: overcoming heterogeneity in drug sensitivity", *Journal of Investigative Dermatology*, vol. 85, no. 1, pp. 43–46, 1985.

[39] M. H. Niemz, *Laser-tissue interactions: fundamentals and applications*, Springer, 2007.

[40] J. C. Hebden, S. R. Arridge, and D. T. Delpy, "Optical imaging in medicine: i. experimental techniques", *Physics in medicine and biology*, vol. 42, no. 5, pp. 825–840, 1997.

[41] F. Gao, H. Zhao, Y. Tanikawa, and Y. Yamada, "Optical tomographic mapping of cerebral haemodynamics by means of time-domain detection: methodology and phantom validation", *Physics in medicine and biology*, vol. 49, no. 6, pp. 1055–1078, 2004.

[42] P. Kiefhaber, G. Nath, and K. Moritz, "Endoscopical control of massive gastrointestinal hemorrhage by irradiation with a high-power neodymium-yag laser", *Progress in surgery*, vol. 15, pp. 140–155, 1977.

[43] R. R. Anderson and J. A. Parrish, "Microvasculature can be selectively damaged using dye lasers: a basic theory and experimental evidence in human skin", *Lasers in surgery and medicine*, vol. 1, no. 3, pp. 263–276, 1981.

[44] M. El-Tonsy, Hany, M. El-Domyati, Mostafa, A. El-Sawy, Esmat, W. El-Din, Hosam, T. E.-D. A.-S. Anbar, and A. Raouf, Hamza, "Continuous-wave Nd:Yag laser hyperthermia: a successful modality in treatment of basal cell carcinoma", *Dermatology online journal*, vol. 10, no. 2, p. 3, 2004.

[45] A. Y. Citkaya and S. S. Seker, "Modeling and simulation of temperature distribution in laser-tissue interaction", *Session 2P7 Computational Electromagnetics, Hybrid Methods*, pp. 844–847, 2011.

[46] A. J. Welch, J. A. Pearce, K. R. Diller, G. Yoon, and W. F. Cheong, "Heat generation in laser irradiated tissue", *Journal of biomechanical engineering*, vol. 111, no. 1, pp. 62–68, 1989.

[47] A. J. Welch, G. Yoon, and M. J. van Gemert, "Practical models for light distribution in laser-irradiated tissue", *Lasers in surgery and medicine*, vol. 6, no. 6, pp. 488–493, 1987.

[48] A. Hofstetter, E. Keiditsch, T. Halldorsson, H. Bulow, and F. Frank, *The neodymium-YAG laser in urology*, Editiones Roche c/o F. Hoffmann-La Roche, 1980.

[49] J. Pearce, "Thermodynamic principles of laser - tissue interaction", In *proceedings of the twelfth annual international conference of the IEEE engineering in medicine and biology society*, pp. 1108–1110, 1990.

[50] A. J. Welch, "Laser irradiation of tissue", In A. Shitzer and R. C. Eberhart (eds.), *Heat transfer in medicine and biology*, Springer US, pp. 135–184, 1985.

[51] C. M. Beacco, S. R. Mordon, and J. M. Brunetaud, "Development and experimental in vivo validation of mathematical modeling of laser coagulation", *Lasers in surgery and medicine*, vol. 14, no. 4, pp. 362–373, 1994.

[52] A. N. Takata, L. Zaneveld, and W. Richter, "Laser-induced thermal damage of skin", Technical report, DTIC Document, 1977.

[53] T. Halldorson and J. Langerholc, "Thermodynamic analysis of laser irradiation of biological tissue", *Applied optics*, vol. 17, no. 24, pp. 3948–3958, 1978.

[54] L. A. Priebe and A. J. Welch, "A dimensionless model for the calculation of temperature increase in biologic tissues exposed to nonionizing radiation", *IEEE Transactions on Biomedical Engineering*, vol. BME-26, no. 4, pp. 244–250, 1979.

[55] L. Cummins and M. Nauenberg, "Thermal effects of laser radiation in biological tissue.", *Biophysical Journal*, vol. 42, no. 1, pp. 99–102, 1983.

[56] T. Halldorson, W. Rother, J. Langerholc, and F. Frank, "Theoretical and experimental investigations prove nd: YAG laser treatment to be safe", *Lasers in surgery and medicine*, vol. 1, no. 3, pp. 253–262, 1981.

[57] M. Motamedi, A. Gonzales, and G. Yoon, "Thermal response of gastro-intestinal tissue to Nd:YAG laser irradiation: A theoretical and experimental investigation.", *LIA*, vol. 37, pp. 80–89, 1983.

[58] S. L. Jacques and S. A. Prahl, "Modeling optical and thermal distributions in tissue during laser irradiation", *Lasers in surgery and medicine*, vol. 6, no. 6, pp. 494–503, 1987.

[59] G. J. Derbyshire, *A dynamic laser-induced thermal ablation model*, Graduate School of Arts and Sciences, University of Pennsylvania, 1989.

[60] L. I. Grossweiner, A. M. al Karmi, P. W. Johnson, and K. R. Brader, "Modeling of tissue heating with a pulsed Nd:YAG laser", *Lasers in surgery and medicine*, vol. 10, no. 3, pp. 295–302, 1990.

[61] V. A. Korolyov and V. V. Grigoryants, "Continuous laser radiation effect at 1.06 um on gastrointestinal tract", *Lasers in Surgery and Medicine*, vol. 10, no. 2, pp. 185–188, 1990.

[62] S. Diaz, G. Aguilar, E. Lavernia, and B. Wong, "Modeling the thermal response of porcine cartilage to laser irradiation", *IEEE Journal of Selected Topics in Quantum Electronics*, vol. 7, no. 6, pp. 944–951, 2001.

[63] S. H. Diaz, J. S. Nelson, and B. J. F. Wong, "Rate process analysis of thermal damage in cartilage", *Physics in Medicine and Biology*, vol. 48, no. 1, pp. 19–29, 2003.

[64] J. Zhou, J. K. Chen, and Y. Zhang, "Theoretical analysis of thermal damage in biological tissues caused by laser irradiation", *Molecular & cellular biomechanics: MCB*, vol. 4, no. 1, pp. 27–39, 2007.

[65] G. W. Yoon, *The thermal effect of laser beam scattering in biological medium*, University of Texas at Austin, 1984.

[66] M. S. Patterson, B. C. Wilson, and D. R. Wyman, "The propagation of optical radiation in tissue i. models of radiation transport and their application", *Lasers in Medical Science*, vol. 6, no. 2, pp. 155–168, 1991.

[67] Z. Gourgouliatos, S. Ghaffari, A. Welch, K. Diller, and R. Straight, "Measurements of argon laser light attenuation in the skin 'in vivo' using a unique animal model", In *Engineering in medicine and biology society, 1989. images of the twenty-first century., proceedings of the annual international conference of the IEEE engineering in*, vol. 6, pp. 1749–1750, 1989.

[68] R. Splinter, R. H. Svenson, L. Littmann, J. R. Tuntelder, C. H. Chuang, G. P. Tatsis, and M. Thompson, "Optical properties of normal, diseased, and laser photocoagulated myocardium at the nd: YAG wavelength.", *Lasers in surgery and medicine.*, vol. 11, no. 2, pp. 117–124, 1991.

[69] P. Parsa, S. L. Jacques, and N. S. Nishioka, "Optical properties of rat liver between 350 and 2200 nm", *Applied optics*, vol. 28, no. 12, pp. 2325–2330, 1989.

[70] M. Kikuchi and Y. Sakurai, "Spectral transmittance and reflectance of living tissues and change of their optical characteristics under Nd:YAG laser irradiation", In Graz (ed.), *3rd International Congress of Laser Surgery*, 1979, Proceedings.

[71] L. J. Steven, "Skin Optics", News, Oregon Medical Laser Center, 1998, omlc.ogi.edu/news/jan98/skinoptics.html.

[72] I. S. Saidi, *Transcutaneous optical measurement of hyperbilirubinemia in neonates*, Rice, University, Houston, TX , USA, 1992.

[73] S. Jacques and D. McAuliffe, "The melanosome: threshold temperature for explosive vaporization and internal absorption coefficient during pulsed laser irradiation.", *Photochemistry and photobiology*, vol. 53, no. 6, pp. 769–775, 1991.

[74] S. L. Jacques, R. D. Glickman, and J. A. Schwartz, "Internal absorption coefficient and threshold for pulsed laser disruption of melanosomes isolated from retinal pigment epithelium", pp. 468–477, 1996.

[75] S. Wray, M. Cope, D. T. Delpy, J. S. Wyatt, and E. O. Reynolds, "Characterization of the near infrared absorption spectra of cytochrome aa3 and haemoglobin for the non-invasive monitoring of cerebral oxygenation", *Biochimica et biophysica acta*, vol. 933, no. 1, pp. 184–192, 1988.

[76] C. R. Simpson, M. Kohl, M. Essenpreis, and M. Cope, "Near-infrared optical properties of ex vivo human skin and subcutaneous tissues measured using the monte carlo inversion technique", *Physics in Medicine and Biology*, vol. 43, no. 9, pp. 2465–2478, 1998.

[77] A. N. Bashkatov, E. A. Genina, V. I. Kochubey, and V. V. Tuchin, "Optical properties of human skin, subcutaneous and mucous tissues in the wavelength range from 400 to 2000 nm", *Journal of Physics D: Applied Physics*, vol. 38, no. 15, p. 2543, 2005.

[78] J. T. J. Walsh and T. F. Deutsch, "Pulsed CO2 laser tissue ablation: measurement of the ablation rate", *Lasers in surgery and medicine*, vol. 8, no. 3, pp. 264–275, 1988.

[79] R. Dua and S. Chakraborty, "A novel modeling and simulation technique of photo–thermal interactions between lasers and living biological tissues undergoing multiple changes in phase", *Computers in biology and medicine*, vol. 35, no. 5, pp. 447–462, 2005.

[80] M. J. Brugmans, J. Kemper, G. H. Gijsbers, F. W. van der Meulen, and M. J. van Gemert, "Temperature response of biological materials to pulsed non-ablative CO2 laser irradiation", *Lasers in surgery and medicine*, vol. 11, no. 6, pp. 587–594, 1991.

[81] F. J. Henriques, "Studies of thermal injury; the predictability and the significance of thermally induced rate processes leading to irreversible epidermal injury", *Archives of pathology*, vol. 43, no. 5, pp. 489–502, 1947.

[82] A. Welch, "The thermal response of laser irradiated tissue", *IEEE Journal of Quantum Electronics*, vol. 20, no. 12, pp. 1471–1481, 1984.

[83] C. E. Fugitt, "A rate process of thermal injury.", Technical Report 606, Armed Forces Special Weapons Project, 1955.

[84] A. M. Stoll and L. C. Greene, "Relationship between pain and tissue damage due to thermal radiation", *Journal of applied physiology*, vol. 14, no. 3, pp. 373–382, 1959.

[85] A. N. Takata, "Development of criterion for Predicting Thermal Injury", *Aerospace Medicine*, vol. 45, pp. 634–637, 1974.

[86] Y. C. Wu, "A modified criterion for predicting thermal injury.", Technical report, National Bureau of Standards, Washington, District of Columbia, 1982.

[87] E. Y. Ng and L. T. Chua, "Mesh-independent prediction of skin burns injury", *Journal of medical engineering & technology*, vol. 24, no. 6, pp. 255–261, 2000.